1 **TITLE**

2 Training-induced bioenergetic improvement in human skeletal muscle is associated with non-
3 stoichiometric changes in the mitochondrial proteome without reorganization of respiratory
4 chain content

5 **AUTHORS**

6 Cesare Granata[1,2,11,*], Nikeisha J. Caruana[2,3,11], Javier Botella[2], Nicholas A. Jamnick[2,4], Kevin
7 Huynh[5], Jujiao Kuang[2], Hans A. Janssen[2], Boris Reljic[3,6], Natalie A. Mellett[5], Adrienne
8 Laskowski[1,7], Tegan L. Stait[7], Ann E. Frazier[7,8], Melinda T. Coughlan[1,9], Peter J. Meikle[5],
9 David R. Thorburn[7,8,10], David A. Stroud[3,12,*] and David J. Bishop[2,12,13,*]

10 **AFFILIATIONS**

11 [1]Department of Diabetes, Central Clinical School, Monash University, Melbourne, VIC,
12 3004, Australia

13 [2]Institute for Health and Sport (IHES), Victoria University, Melbourne, VIC, 3011, Australia

14 [3]Department of Biochemistry and Pharmacology and Bio21 Molecular Science and
15 Biotechnology Institute, The University of Melbourne, Parkville, VIC, 3010, Australia

16 [4]Metabolic Research Unit, School of Medicine and Institute for Mental and Physical Health
17 and Clinical Translation (iMPACT), Deakin University, Geelong, VIC, Australia

18 [5]Metabolomics Laboratory, Baker Heart & Diabetes Institute, Melbourne, VIC, 3004,
19 Australia

20 [6]Current address: Department of Biochemistry and Molecular Biology, Monash Biomedicine
21 Discovery Institute, Monash University, 3800, Melbourne, Australia.

22 [7]Murdoch Children's Research Institute, Royal Children's Hospital, Melbourne, VIC, 3052,

23 Australia

24 [8]Department of Paediatrics, The University of Melbourne, Melbourne, VIC, 3052, Australia

25 [9]Baker Heart & Diabetes Institute, Melbourne, VIC, 3004, Australia

26 [10]Victorian Clinical Genetics Services, Royal Children's Hospital, Melbourne, VIC, 3052,

27 Australia

28 [11]Co-first author

29 [12]Co-senior author

30 [13]Lead contact

31 ***Correspondence:** cesare.granata@monash.edu - cesare.granata@ddz.de (C.G.),

32 david.stroud@unimelb.edu.au (D.A.S), david.bishop@vu.edu.au (D.J.B)

SUMMARY

Mitochondrial defects are implicated in multiple diseases and aging. Exercise training is an accessible and inexpensive therapeutic intervention improving mitochondrial bioenergetics and quality of life. By combining a multi-omics approach with biochemical and *in silico* normalization, we removed the bias arising from the training-induced increase in human skeletal muscle mitochondrial content to unearth an intricate and previously undemonstrated network of differentially prioritized mitochondrial adaptations. We show that changes in hundreds of transcripts, proteins, and lipids are not stoichiometrically linked to the increase in mitochondrial content. We demonstrate that enhancing electron flow to oxidative phosphorylation (OXPHOS) is more important to improve ATP generation than increasing the abundance of the OXPHOS machinery, and that training-induced supercomplex formation does not confer enhancements in mitochondrial bioenergetics. Our study provides a new analytical approach allowing unbiased and in-depth investigations of training-induced mitochondrial adaptations, challenging our current understanding and calling for careful reinterpretation of previous findings.

48 **INTRODUCTION**

49 Mitochondria are the main site of energy conversion in the cell and have critical roles in other
50 important biological processes (Spinelli and Haigis, 2018). Owing to this, defects in
51 mitochondria have been implicated in multiple diseases, medical conditions, and aging
52 (Gorman et al., 2016; Lin and Beal, 2006; López-Otín et al., 2013; Nunnari and Suomalainen,
53 2012). The development of interventions to improve the content and function of mitochondria
54 is therefore essential to enhance quality of life and to extend life expectancy.

55 Exercise training is one of the most widely accessible interventions or "therapies" to
56 stimulate mitochondrial biogenesis (Holloszy, 1967; Hoppeler et al., 1973). As arguably the
57 most extensive and also natural perturbation, exercise is also an excellent experimental model
58 for understanding both the complex nature of mitochondrial biogenesis and the plasticity of
59 the skeletal muscle mitochondrial proteome in humans (Neufer et al., 2015). It is well
60 accepted that exercise training induces an increase in mitochondrial content and respiratory
61 function in human skeletal muscle (Granata et al., 2018b). However, our knowledge of
62 mitochondrial adaptations is limited to a small fraction of the mitochondrial proteome
63 (Granata et al., 2018a), and is complicated by large training-induced changes in
64 mitochondrial content, which limit the ability to interpret adaptations in individual proteins
65 independent of the overall change in mitochondrial content. To account for this, most studies
66 to date have either performed analyses in mitochondrial isolates obtained after differential
67 centrifugation or have employed a crude normalization strategy involving the use of markers
68 of mitochondrial content, such as citrate synthase (CS) activity (Granata et al., 2018b;
69 Groennebaek et al., 2020). Nonetheless, due to limitations in both approaches (Franko et al.,
70 2013; Groennebaek et al., 2020), there remain major gaps in our understanding of the
71 magnitude, timing, and direction of change in individual mitochondrial proteins and related
72 functional pathways, independent of the overall change in mitochondrial content.

73 A key biological function of mitochondria is energy conversion via oxidative
74 phosphorylation (OXPHOS), which is carried out by the four multi-protein complexes
75 (complexes I to IV [CI-CIV]) of the electron transport chain (ETC) and F_0F_1-ATP synthase
76 (or CV) (Pesta and Gnaiger, 2012). Assembly of the OXPHOS complexes is an intricate
77 process requiring the coordination of two genomes (nuclear and mitochondrial) and non-
78 subunit proteins known as assembly factors (Signes and Fernandez-Vizarra, 2018). Only two
79 studies have investigated training-induced changes in OXPHOS complexes in humans
80 (Greggio et al., 2017; Wyckelsma et al., 2017), reporting that exercise differentially
81 modulates the assembly and composition of respiratory chain complexes - including their
82 high molecular weight supercomplex (SC) assemblies. Furthermore, no study has
83 investigated if training-induced changes in chaperones, assembly factors, and single
84 OXPHOS subunits occur in conjunction with, or precede, changes in the complete, functional
85 complexes. Many other processes support assembly and maintenance of the OXPHOS
86 complexes, including mitochondrial protein import and assembly pathways, mitochondrial
87 DNA transcription and translation, metabolite carriers, and pathways producing critical
88 cofactors such as coenzyme Q and iron-sulphur proteins (Fe-S) (Signes and Fernandez-
89 Vizarra, 2018). In turn, these processes are reliant on pathways supporting mitochondrial
90 biogenesis more broadly, such as lipid biogenesis and maintenance of mitochondrial
91 morphology. Whether these processes and pathways are activated by exercise training and at
92 which specific times remains unknown.

93 Here, we employed a 3-phase training intervention, combined with a multi-omics approach
94 (transcriptomics, proteomics, and lipidomics) and a newly developed normalization strategy
95 that removed the bias induced by large alterations in mitochondrial content, to investigate
96 mitochondrial adaptations in human skeletal muscle. Our findings revealed an intricate and
97 timely remodeling in the mitochondrial transcriptome, proteome, and lipidome, independent

98 of changes in overall mitochondrial content. Post-normalization, we identified 185
99 differentially expressed mitochondrial proteins, representing multiple protein functional
100 classes, as well as bioenergetic and metabolic pathways, that followed distinct patterns of
101 adaptation. In addition, we provide evidence that training-induced changes in the abundance
102 and/or organization of SCs do not contribute to improvements in mitochondrial bioenergetics.
103 Our study provides a new analytical approach that expands our fundamental understanding of
104 training-induced mitochondrial biogenesis. It challenges our current knowledge and calls for
105 careful reinterpretation of previous findings, while leading to new hypotheses on how
106 training alters mitochondrial protein content and function, thus providing an important
107 resource with implications for both health and disease.

108 **RESULTS AND DISCUSSION**

109 ***Increases in mitochondrial content underlie changes in markers of mitochondrial***
110 ***biogenesis and mitochondrial respiratory function following training.*** The traditional view
111 of mitochondrial biogenesis suggests that changes in individual mitochondrial proteins are
112 stoichiometrically linked to changes in mitochondrial content. Although this has been
113 questioned previously (Ørtenblad, 2018), it remains an unresolved matter. To challenge this
114 paradigm, we employed an experimental model in which ten men were sequentially exposed
115 to different volumes (normal- [NVT], high- [HVT] and reduced- [RVT] volume training) of
116 high-intensity interval training (HIIT) with biopsies taken at baseline (BL) and post-NVT
117 (PN), post-HVT (PH) and post-RVT (PR) (Figure 1A). This design was chosen as we have
118 previously demonstrated that changes (increases or decreases) in training volume lead to
119 changes in mitochondrial content and markers of mitochondrial biogenesis (Bishop et al.,
120 2019; Bishop et al., 2014; Granata et al., 2018b; Granata et al., 2016a). Weekly training
121 volumes for the three phases are shown in Figure 1B; changes in physiological and
122 performance parameters are presented in Table 1.

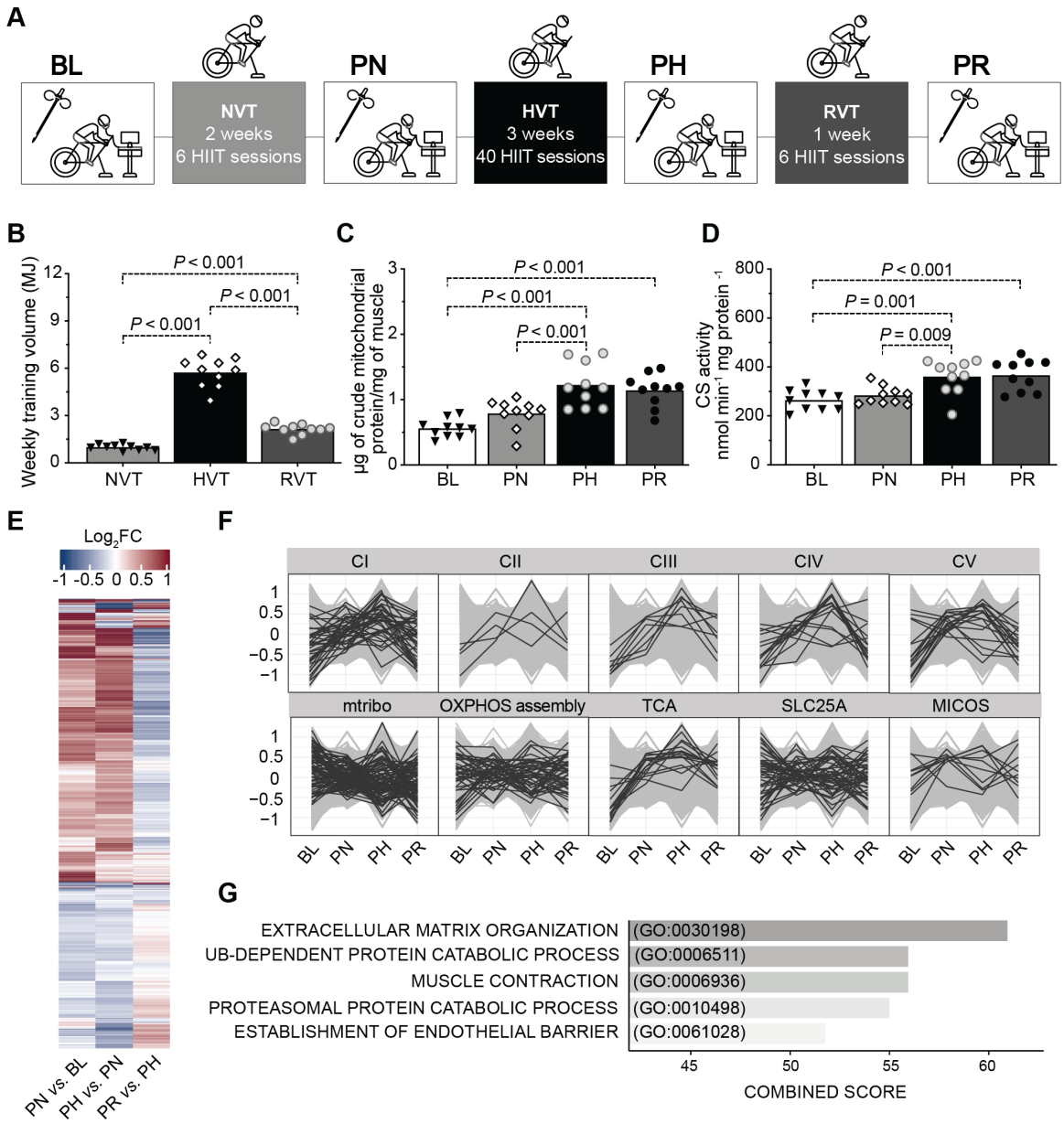

Figure 1. RNA-seq highlights a complex network of transcriptional responses underpinning the training-induced increases in markers of mitochondrial content in human vastus lateralis muscle

(A) Study design; colored boxes indicate a training phase: NVT (normal-volume training), HVT (high-volume training), and RVT (reduced-volume training), whereas open boxes indicate a testing session and resting skeletal muscle biopsy: baseline (BL), post-NVT (PN), post-HVT (PH), and post-RVT (PR)

(B) Weekly training volume during the NVT, HVT, and RVT training phase; training volume was calculated by multiplying the absolute exercise intensity in Watts by the effective duration of exercise training in minutes (excluding the warm up and the rest periods between intervals) by the total number of training sessions in each phase.

135 (C) Mitochondrial yield per mg of tissue achieved during mitochondria isolation of human
136 vastus lateralis biopsy samples (biochemical enrichment of mitochondrial protein).
137 (D) Citrate synthase (CS) enzyme activity assessed in whole-tissue (vastus lateralis)
138 homogenates.
139 (E) Heatmap of differentially expressed transcripts between training phases determined with
140 an adjusted $P < 0.05$ (Benjamini Hochberg). Row clustering determined by unsupervised
141 hierarchical cluster analysis.
142 (F) Profile plots showing relative scaled transcripts of subunits of the five oxidative
143 phosphorylation (OXPHOS) complexes (CI to CV), mitochondrial ribosomes (mtribo),
144 OXPHOS assembly, TCA cycle, SLC25As and mitochondrial contact site and cristae organising
145 system (MICOS) complex. Transcripts grouped according to known literature (see methods).
146 (G), Biological process (BP) gene ontology of all differentially expressed transcripts as in
147 (E); the five terms with the highest combined score, as determined by *Enrichr* (see methods),
148 are displayed.
149 HIIT: high-intensity interval training; MJ: megajoules; CI-V: complex I to V; IB:
150 immunoblotting; ▼,◊,○, and ● represent individual values; bars represent mean values.
151 Datasets (B), (C), and (D) were analyzed by repeated measures one-way ANOVA followed
152 by Tukey's post hoc testing; n = 10; significance: $P < 0.05$. Dataset (E), (F), and (G) n = 5.

153 **Table 1**. Participants' physiological and endurance performance measurements before and
154 after each training phase

Measurement	BL	PN	PH	PR
Age	22.3 ± 5.2			
Height	178.1 ± 10.7			
Body mass	78.8 ± 12.1	79.0 ± 12.9	78.0 ± 12.5	77.9 ± 11.8$^{\#}$
BMI	24.8 ± 2.9	24.9 ± 3.2	24.6 ± 3.0	24.5 ± 2.9$^{\#}$
$\dot{V}O_{2Peak}$	46.7 ± 8.2	47.7 ± 8.8	50.5 ± 6.0$^{*\#}$	50.0 ± 6.0*
$\dot{W}_{LT}$	174.1 ± 30.7	182.5 ± 33.0	222.2 ± 36.2$^{*\#}$	219.6 ± 31.4$^{*\#}$
$\dot{W}_{peak}$	231.1 ± 43.2	233.2 ± 43.5	266.3 ± 42.4$^{*\#}$	264.5 ± 40.4$^{*\#}$
20k-TT time	2321.0 ± 168.1	2309.1 ± 257.4	2094.6 ± 130.8$^{*\#}$	2030.1 ± 140.5$^{*\#}$

155 BL: baseline; PN: post normal-volume training; PH: post high-volume training; PR: post
156 reduced-volume training; BMI: body mass index [kg m^{-2}]; $\dot{V}O_{2Peak}$: peak oxygen uptake [mL
157 min^{-1} kg^{-1}]; $\dot{W}_{LT}$: power at the lactate threshold [Watts]; $\dot{W}_{peak}$: peak power output [Watts];
158 20k-TT: 20-km time trial [seconds]. All values are mean ± SD; n = 10 for all analyses; all
159 datasets analysed by repeated measures one-way ANOVA followed by Tukey's post hoc
160 testing. Significantly different ($P < 0.05$) * *vs.* BL, # *vs.* PN.

161 We first verified that changes in training volume induced changes in the yield of
162 mitochondrial proteins isolated from muscle biopsies (Figure 1C), and citrate synthase (CS)
163 activity (Figure 1D) - a commonly used biomarker of mitochondrial content (Larsen et al.,
164 2012), as previously reported (Barnard et al., 1970; Egan et al., 2011; Granata et al., 2018b;
165 Granata et al., 2016a; Holloszy, 1967; Morgan et al., 1971). We then confirmed that classic
166 markers of mitochondrial biogenesis, such as the protein content of OXPHOS subunits
167 assessed in whole-muscle lysates (Figure S1A, upper panels), as well as measurements of
168 mitochondrial respiratory function, such as mitochondrial respiration in permeabilized fibers
169 and ETC enzyme activity (Figure S1B, and C, respectively, all upper panels) changed, for the
170 most part, as a consequence of changes in training volume. RVT resulted in no change in any
171 of these markers, suggesting that the training stimulus was sufficient to prevent a decrease in
172 these parameters. Subsequently, to investigate the underpinnings of training-induced changes
173 in the above markers, we normalized these values by CS activity, a widely-used
174 normalization strategy to account for differences in mitochondrial content (Granata et al.,
175 2018b; Granata et al., 2016a; Larsen et al., 2012; Meinild Lundby et al., 2018). This
176 demonstrated that, for the most part, absolute changes in markers of mitochondrial biogenesis
177 and respiratory function were stoichiometrically associated with the overall increase in
178 mitochondrial content (Figure S1A, B, and C, all lower panels).

179 ***Disentangling changes in the mitochondrial proteome from the general increase in***
180 ***mitochondrial content observed post-training.*** The above findings seem to indicate that
181 altering training volume results in a stoichiometric relationship between training-induced
182 changes in mitochondrial content and markers of mitochondrial biogenesis and mitochondrial
183 respiratory function (Granata et al., 2018b). However, whether there is also a fixed
184 stoichiometry between changes in mitochondrial content and individual mitochondrial
185 proteins, protein functional classes and metabolic pathways, remains undetermined. To test
186 this, we first employed RNA sequencing (RNA-seq) based transcriptomics (Table S1). We
187 identified 1206 differentially expressed transcripts (Figure 1E, Table S2), and we observed
188 the expected increase in gene transcripts encoding subunits of the OXPHOS complexes
189 (Figure 1F, upper panels, compare with Figure S1A, upper panels) and enzymes of the
190 tricarboxylic acid (TCA) cycle (Figure 1F, central lower panel), consistent with previous
191 studies in humans (Pillon et al., 2020). However, transcripts for genes encoding other
192 mitochondrial proteins did not all follow the same trend (Figure 1F, lower panels). Moreover,
193 gene ontology enrichment analysis of all differentially expressed transcripts did not identify
194 significant alterations of pathways involved in mitochondrial respiratory function (Figure
195 1G), despite the increase in mitochondrial respiration and ETC enzyme activity reported
196 above (Figure S1B and C, respectively). This reveals a greater complexity in the
197 transcriptional responses to exercise than previously hypothesized; i.e., not all mitochondria-
198 related gene transcripts changed in the same direction and with a similar magnitude following
199 different training phases (Figure 1F).

200 As transcriptomics suggested there may not be a fixed stoichiometry between training-
201 induced changes in mitochondrial content and individual mitochondrial proteins, we sought
202 to support these findings with quantitative proteomics. To negate the general increase in
203 mitochondrial content following exercise training (Figure 1D) and to avoid this inherent bias

204 on our proteomics measurements, we performed label-free quantitative (LFQ) proteomics on
205 equal amounts of mitochondria-enriched fractions (biochemical enrichment of mitochondrial
206 proteins using differential centrifugation). We quantified 1,411 proteins - 726 of which were
207 annotated as mitochondrial based on either the Mitocarta2.0 (Calvo et al., 2016) or the
208 Integrated Mitochondrial Protein Index (IMPI; Known and Predicted Mitochondrial) (Smith
209 and Robinson, 2019) databases (Table S3). Considering only the high-confidence IMPI
210 (Known Mitochondrial) dataset, mitochondrial proteins represented 41% of the total number
211 of proteins identified in our mitochondria-enriched fraction (584 annotated mitochondrial
212 proteins), contributing to 32% of the overall protein abundance based on raw intensity data
213 for each protein (Table S3). This demonstrated the presence of a significant proportion of co-
214 isolating non-mitochondrial proteins, with enrichment analysis indicating these to be
215 predominantly of myofibrillar origin (Figure S2A), consistent with most mitochondria in
216 skeletal muscle being tightly associated with myofibrils (Egan et al., 2011). Surprisingly, we
217 still observed a relative increase in the abundance of mitochondrial proteins within isolates
218 following training (Figure 2A, upper panel, magenta profiles), an artefact that likely stems
219 from differences in mitochondrial protein enrichment (MPE) - the contribution of
220 mitochondrial protein intensities in biochemically isolated mitochondria relative to all protein
221 intensities - at different time points. Indeed, the MPE for the 4 different time points in the
222 present study was significantly different (Figure 2A, middle panel) and corresponded to
223 24.5% at baseline (BL), 31.5% post-NVT (PN), 39.3% post-HVT (PH), and 34.5% post-RVT
224 (PR) (Table S3) - a pattern consistent with our assessment of mitochondrial content (compare
225 Figure 2A, middle panel with Figure 1C and D).

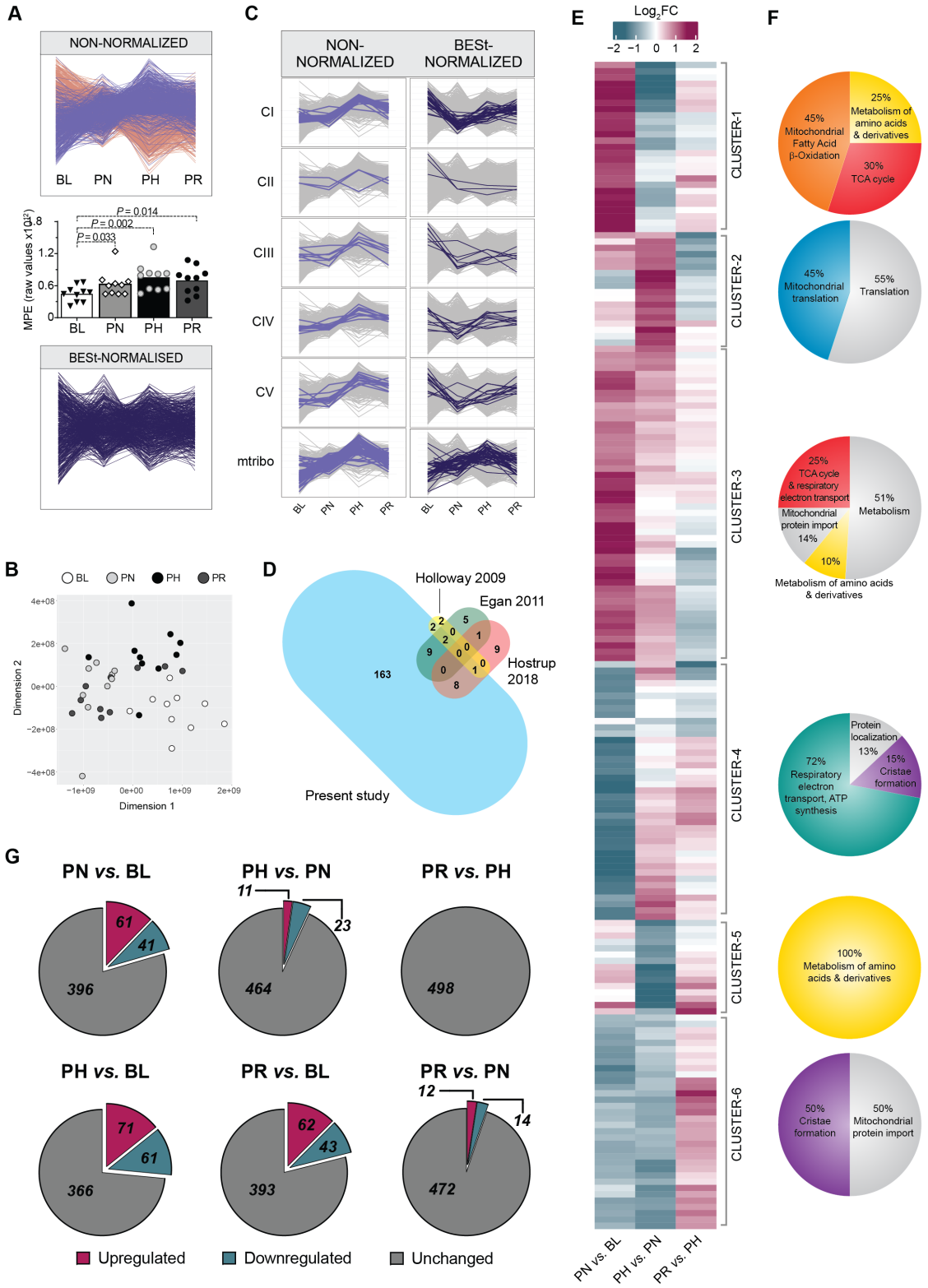

Figure 2. Correcting for training-induced changes in mitochondrial content reveals differentially expressed protein clusters with divergent prioritization in response to training

(A) Training-induced differences in the mitochondrial protein content of isolated mitochondrial (IM) fractions obtained from vastus lateralis muscle biopsies. Upper panel:

232 profile plot of all non-normalized intensity values displaying "known mitochondrial" (IMPI
233 "Known Mitochondrial") (magenta) and non-mitochondrial (salmon) proteins co-
234 precipitating during mitochondrial isolation. Proteins identified in less than 70% of samples
235 were removed. Middle panel: mitochondrial protein enrichment (MPE) obtained by adding
236 the raw intensity values from LC-MS/MS analysis of all "known mitochondrial" proteins
237 (IMPI "Known Mitochondrial") at the four different time points. ▼,◊,○, and ● represent
238 individual values; bars represent mean values; analyzed by repeated measures one-way
239 ANOVA followed by Tukey's post hoc testing. Significance: $P < 0.05$. Lower panel: same as
240 upper panel but following removal of non-mitochondrial proteins and statistical correction
241 (BESt-) normalization.
242 (B) Multidimensional scaling analysis showing segregation of samples obtained from IM
243 fractions of BESt-normalized proteomics values.
244 (C) Scaled profile plots showing the relative abundance of subunits of OXPHOS complexes
245 and mtribo of the non-normalized intensity values of "known mitochondrial" proteins (IMPI
246 "Known Mitochondrial") following valid value filtering (left panels), and values obtained
247 after BESt-normalization (right panels).
248 (D) Venn diagram representing the overlap in differentially expressed proteins between the
249 present study and previous literature utilizing young healthy humans (Egan et al., 2011;
250 Holloway et al., 2009; Hostrup et al., 2018). The bubble size for each study is proportional to
251 the number of differentially expressed proteins identified (this was not possible for the
252 overlapping size).
253 (E) Heatmap of BESt-normalized differentially expressed mitochondrial proteins (IMPI
254 "Known Mitochondrial"), determined with an adjusted $P < 0.01$ (Benjamini Hochberg). Row
255 clustering determined by unsupervised hierarchical cluster analysis.
256 (F) Venn diagram representation of the gene ontology of the six clusters identified in (E) obtained
257 from enrichment analysis (using the ClueGO [v2.5.6] application in Cytoscape [v3.7.1]; see
258 methods) of all proteins belonging to each cluster performed separately (Table S5).
259 (G) Venn diagram representations of the number of BESt-normalized differentially expressed
260 mitochondrial proteins (IMPI "Known Mitochondrial") between each of the time points.
261 Differentially expressed proteins for each time point comparison were identified by linear
262 modelling with an adjusted P value < 0.01 using the Benjamini Hochberg method, as shown
263 in Table S7.
264 BL: baseline; PN: post-NVT; PH: post-HVT; PR: post-RVT. n = 5 for **a**, **b**, and **c**, n = 10 for
265 all other analyses.

266 The above findings highlight that the standard approach of relying on biochemical
267 enrichment to eliminate the bias arising from different MPEs across time points is insufficient
268 and that an additional strategy is needed. We therefore complemented our biochemical
269 enrichment approach with a novel statistical correction strategy consisting of *i*) removing
270 proteins that were identified in less than 70% of samples, *ii*) removing all except high-
271 confidence mitochondrial proteins (IMPI Known Mitochondrial), and *iii*) undertaking
272 variance stabilizing normalization (VSN) (see methods for more detail). This resulted in the
273 retention of 498 mitochondrial proteins normalized across the dataset with high confidence
274 (Table S4). Unlike CS activity, which is a single value for each sample, our normalization
275 strategy utilizes the trends of hundreds of proteins and reduces the confounding effect of
276 potential outliers. This is extremely important, given that previous studies have shown a > 5-
277 fold difference in training-induced synthesis rate between fast and slow synthesized
278 mitochondrial proteins in human skeletal muscle (Groennebaek et al., 2020; Scalzo et al.,
279 2014; Shankaran et al., 2016). Plotting the resulting data revealed that the general increase in
280 mitochondrial proteins with different training volumes had been compensated for, indicating
281 that our biochemical enrichment and statistical correction (BESt-normalization) was
282 successful (Figure 2A, lower panel). In further support of our normalization strategy,
283 multidimensional scaling analysis showed good segregation of samples corresponding to the
284 different time points (Figure 2B).

285 To assess the power of our normalization strategy, we compared results from non-normalized
286 and BESt-normalized proteomics values. Whereas analysis of non-normalized intensity
287 values revealed a lack of change in the abundance of OXPHOS and mitochondrial ribosomal
288 subunits post-NVT, followed by a marked increase post-HVT, and a decrease post-RVT
289 (Figure 2C, left panels), results from BESt-normalized values showcased a very different
290 picture, as the content of OXPHOS subunits was markedly decreased (deprioritized) post-

291 NVT, and showed discreet and specific changes (mainly modest increases) thereafter (Figure
292 2C, right panels; results discussed in more detail later), whereas mitochondrial ribosomal
293 subunits increased to a greater extent than mitochondrial content (prioritized) (Figure 2C,
294 right panels). These findings demonstrate the power of our BESt-normalization strategy
295 compared to classical approaches, as it enables the first unbiased comparison of the changes
296 in individual mitochondrial proteins relative to the overall increase in mitochondrial content
297 following training, providing clear evidence that these changes are not stoichiometrically
298 linked. As a means of comparison, we also employed the classical approach of normalizing
299 the abundances of specific proteins derived from SDS-PAGE and immunoblot analysis on
300 isolated mitochondrial fractions by CS activity; this demonstrates that while this widely used
301 approach partially corrects for changes in MPE it fails to recapitulate most of the findings
302 observed with our BESt-normalization strategy (Figure S2B).

303 From this point onwards, unless specified otherwise, post BESt-normalization proteomics
304 results will be presented, enabling the investigation of training-induced changes in
305 mitochondrial proteins without the confounding influence of changes in mitochondrial
306 content.

307 ***Discovery of novel mitochondrial proteins and functional classes and metabolic pathways***
308 ***differentially affected by exercise training.*** We next interrogated our BESt-normalized
309 mitochondrial proteome to gain new insights into non-stoichiometric changes in individual
310 mitochondrial proteins following three training phases designed to induce different effects on
311 mitochondrial biogenesis. Using an ANOVA, we identified 185 mitochondrial proteins that
312 were differentially expressed across the three training phases (Table S5). This is ~10-fold
313 greater than the number of proteins reported to change post-training in previous human
314 skeletal muscle studies (Egan et al., 2011; Holloway et al., 2009; Hostrup et al., 2018;

315 Robinson et al., 2017) (Figure 2D). Unsupervised hierarchical clustering of all differentially
316 expressed mitochondrial proteins revealed six clusters (Figure 2E) with distinct patterns of
317 change in response to training (Figure S2C), which also confirmed the absence of a fixed
318 stoichiometry between training-induced changes in mitochondrial content and mitochondrial
319 protein functional classes.

320 Enrichment analysis of differentially expressed proteins within each of the six clusters
321 revealed them to be enriched in, but not always exclusively contain, proteins involved in fatty
322 acid β-oxidation (FAO), mitochondrial translation, the TCA cycle, OXPHOS, metabolism of
323 amino acids, and cristae formation, respectively (Figure 2F; Table S5). Because not all
324 proteins belonging to each individual Reactome pathway segregated within one cluster
325 (Figure S2D), we compared our 185 differentially expressed proteins with proteins belonging
326 to the six aforementioned functional classes (Reactome R-HSA) and other related pathways;
327 matching proteins (Table S6) were used to generate the individual pathway heatmaps
328 presented in Figure 3 and to discuss our findings. In addition, because Reactome, like other
329 protein databases, only provides an extensive but not exhaustive list of proteins involved in
330 each pathway, we complemented our heatmaps with other proteins identified through
331 literature (see methods for more information on how pathways in Table S6 and Figure 3 were
332 generated).

333 To pinpoint the origin of training-induced changes in individual mitochondrial proteins, we
334 performed unpaired t-tests between group pairs following permutation-based false discovery
335 rate (FDR) correction. Using a conservative approach, we matched the differentially
336 expressed proteins identified by each t-test comparison with the 185 differentially expressed
337 proteins identified by the ANOVA (Table S7). The majority of changes occurred during the
338 initial NVT phase (Figure 2G; Table S7), where 102 proteins were differentially expressed,

339 suggesting that the greatest number of mitochondrial adaptations took place within the first
340 few training sessions and these became harder to obtain as the training progressed (Figure 2E,
341 note the strongest changes are found in the "PN *vs.* BL" column). Our study also confirms
342 that the training stimulus during the RVT phase was sufficient to prevent a loss of adaptation
343 (Figure 2G; Table S7).

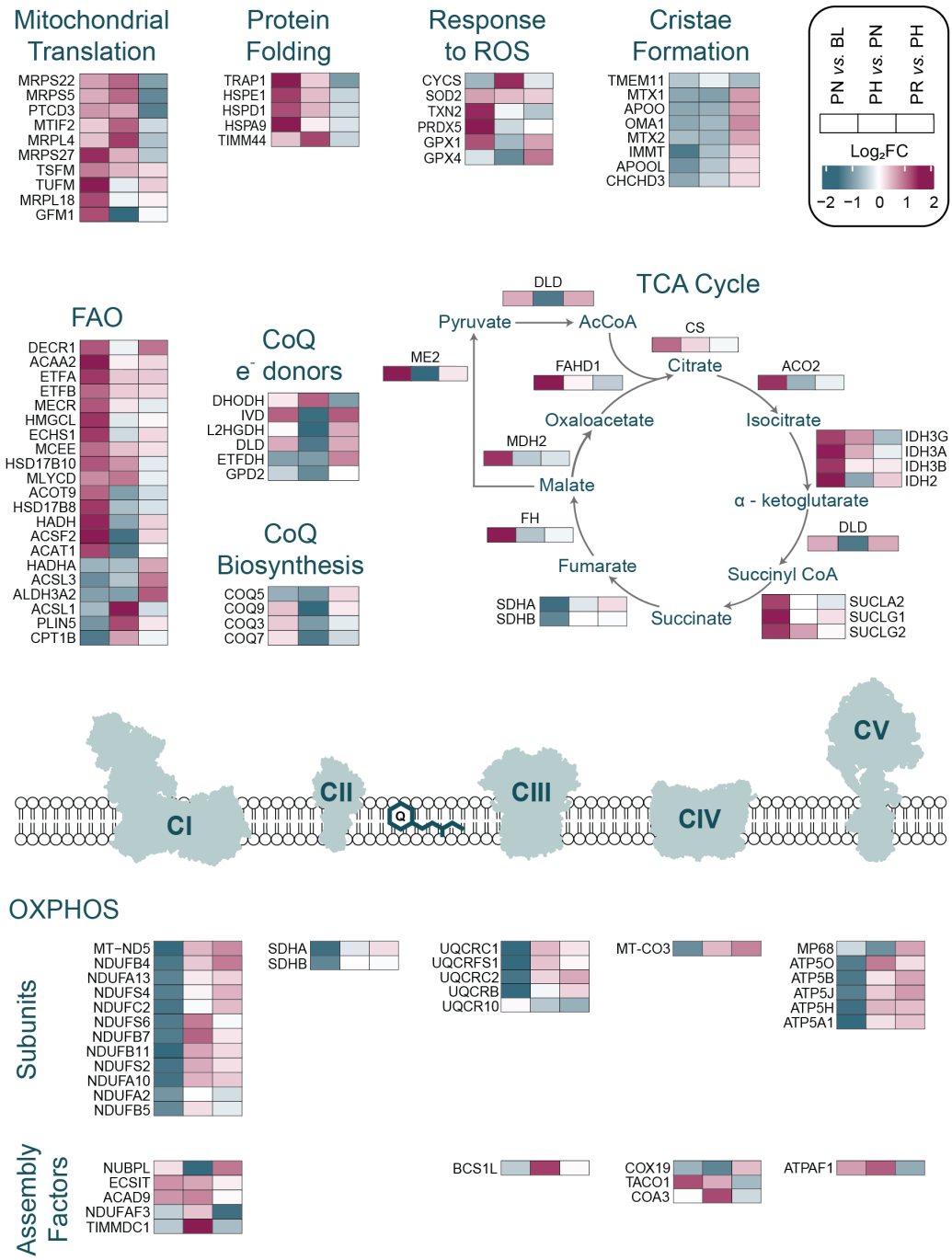

344

345 **Figure 3. Overview of training-induced changes in mitochondrial protein functional**
346 **classes and metabolic pathways**
347 Protein functional classes and/or metabolic pathways (defined in Table S6) as determined in
348 Table S7. Row clustering determined by unsupervised hierarchical cluster analysis. BL:
349 baseline; PN: post-NVT; PH: post-HVT; PR: post-RVT; ROS: reactive oxygen species;
350 FAO: fatty acid β-oxidation; CoQ: Coenzyme Q; TCA: tricarboxylic acid cycle; OXPHOS:
351 oxidative phosphorylation.

352 ***Proteins important for the translation of mitochondrial proteins are sensitive to training***
353 ***volume.*** We next examined the six over-represented pathways highlighted by our enrichment
354 analysis, beginning with the pathway related to mitochondrial protein translation (Figure 3),
355 which mostly segregated within cluster-2 (Figure 2F, and S2D; Table S5). Specifically, we
356 identified proteins from both the small 28S (MRPS5, MRPS22, MRPS27) and large 39S
357 (MRPL4, MRPL18) subunits of the mitochondrial ribosome, as well as proteins involved in
358 translation initiation (MTIF2) and elongation (GFM1, PTCD3, TSFM, TUSM) (Figure 3).
359 Whereas only four proteins were upregulated post-NVT, eight of the 10 aforementioned
360 proteins were upregulated post-HVT, with six remaining elevated post-RVT (Table S7). This
361 is the first study to directly demonstrate training-induced changes in these or related
362 mitochondrial translation proteins in young, healthy humans, as previous research reported
363 training-induced increases in older (65 to 80 years), but not younger (18 to 30 years),
364 individuals (Robinson et al., 2017). Our findings also indicate that changes in proteins
365 involved in mitochondrial protein translation are sensitive to training volume, consistent with
366 a study observing a positive association between these proteins and physical activity levels in
367 healthy individuals (20 to 87 years) (Ubaida-Mohien et al., 2019).

368 ***Mitochondria prioritize the TCA cycle and FAO in response to NVT.*** Proteins involved in
369 the TCA cycle pathway grouped mainly within cluster-3 and, to a lesser extent, cluster-1
370 (Figure 2F and S2D; Table S5). This pathway was characterized by a large and concerted

371 increase post-NVT (12 of 16 enzymes were significantly increased), with many of these
372 proteins remaining upregulated compared to BL both post-HVT and post-RVT (Figure 3,
373 Table S7). Of note, SDHA and SDHB, subunits of CII - the only TCA cycle enzyme that also
374 participates in the ETC - clustered with the majority of OXPHOS subunits (discussed below)
375 and decreased during NVT. While training-induced changes in some TCA cycle proteins
376 have been reported (Egan et al., 2011; Hostrup et al., 2018), this is the first study to reveal
377 training-induced increases in ACO2, SUCLG1, SUCLG2, SUCLA2, and FAHD1, and that
378 these enzymes adapted mostly in a coordinated fashion.

379 Proteins involved in FAO segregated mainly within cluster-1 and cluster-3 (Figure 2F and
380 S2D; Table S5). Our data demonstrated a large and concerted increase in these proteins post-
381 NVT, with minimal (HVT) and no (RVT) changes thereafter (Figure 3; Table S7). Proteins
382 increased post-NVT included chain shortening enzymes involved in FAO (ACAA2, ACSF2,
383 ECHS1, HADH, HSD17B10, MECR, MLYCD) and enzymes required to convert unsaturated
384 fatty acids into intermediates of FAO (DECR1 and HSD17B8). Similar increases were also
385 observed for ETFA and ETFB, which transfer electrons produced during FAO to the
386 OXPHOS system, further highlighting the early increase in FAO. HMGCL and ACAT1, two
387 enzymes involved in the ketogenesis pathway, were also increased, possibly suggesting that
388 excess acetyl-CoA generated by enhanced FAO may be fed into ketogenesis. Taken together,
389 these findings indicate that the synthesis of proteins involved in both the TCA cycle and FAO
390 pathways is prioritized in the early stages of an endurance training intervention; these
391 increases may have contributed, at least in part, to the training-induced increase in
392 mitochondrial respiration (Figure S1B, upper panels).

393 ***Lipidomics highlights a divergent response to training of different lipid classes***. To
394 highlight specific changes in fatty acid composition, LC-MS/MS based comparative

395 lipidomics was performed using the same mitochondrial isolates used for proteomics. A total
396 of 779 species representing 30 lipid classes (Table S8) were quantified. Indeed, changes in
397 the mitochondria-specific cardiolipins (CLs), the biomarker most strongly associated with
398 mitochondrial content in human skeletal muscle (Larsen et al., 2012), mirrored changes in
399 training volume and in non-normalized mitochondrial proteins (compare Figure 4A, left panel
400 with Figure 2A, upper panel; Table S8). Therefore, to ensure that our lipidomics data were
401 corrected for changes in MPE in our fractions, we applied a similar approach to the one used
402 for proteomics where lipidomic results were normalized according to the trend observed for
403 the CL class (see methods). Post-normalization profile plots of CL species indicated that,
404 despite changes in individual CL species, the general increase in mitochondrial content with
405 different training volumes had been compensated for by our normalization strategy (Figure
406 4A; right panel), and the lipid profiles could be used to readily segregate samples across
407 different time points (Figure 4B). From this point on we will present post-normalization
408 lipidomics results, unless specified otherwise.

409 We identified 182 differentially expressed lipid species (Figure 4C; Table S9). Similar to
410 what we observed in our proteomics dataset, and consistent with previous research in humans
411 (Dube et al., 2011; Shepherd et al., 2017), our study highlighted the divergent response to
412 training of different lipid classes and species relative to overall changes in mitochondrial
413 content (Figure 4D). However, in contrast to proteomics, where the greatest number of
414 changes were observed early (during NVT) and no changes were observed during RVT, our
415 lipidomics assessment showed the most significant changes to occur during the latter two
416 stages (Figure S3). This suggests a delayed response to changes in lipid content compared to
417 proteins, and may reflect overall mitochondrial biogenesis as training-induced changes in
418 lipid species were mainly related to mitochondrial membrane-based lipids (CLs,
419 phosphatidylethanolamines and phosphatidylcholines) and the triglycerides (TGs) (Figure

420 S3). Contrary to previous training studies in obese humans (Bruce et al., 2006; Dube et al.,
421 2011; Shepherd et al., 2017), we did not observe reductions in muscle ceramides [with the
422 exception of Cer(d18:1/18:0) during HVT] or diacylglycerol content in our healthy, young
423 men following training. While this could indicate a different response of lipid species in
424 mitochondria isolates (our study) compared to whole-muscle lysates (Bruce et al., 2006;
425 Dube et al., 2011; Shepherd et al., 2017), as previously suggested (Perreault et al., 2018), it
426 could also highlight adaptation differences between obese and healthy individuals.

427 Of relevance to the increase in FAO reported above, we observed a post-NVT decrease in
428 TGs (Figure 4D), a class of lipids used as an important source of energy production during
429 exercise (Goodpaster and Kelley, 1998); however, likely due to the high number of multiple
430 comparisons in our bioinformatic analysis (n = 779), no significant changes in single TG
431 species were detected (Figure S3). The decrease in TGs in our study is consistent with an
432 increase in fatty acid turnover, and is corroborated by the post-NVT increase in FAO
433 enzymes (Figure 3). Finally, changes in TGs (Figure 4D), which are not found in
434 mitochondria but rather in lipid droplets (Walther and Farese Jr, 2012), mirrored changes in
435 PLIN5 (Figure 3). Since PLIN5 is a protein that tethers mitochondria to lipid droplets and
436 regulates the release of lipids for FAO (Benador et al., 2019; Wang et al., 2011), we
437 hypothesize that training-induced changes in TGs may reflect increased association of lipid
438 droplets with mitochondria. While few studies have evaluated the effects of different training
439 interventions on skeletal muscle lipid species, our results add to the growing evidence that
440 changes with training are specific to the exercise prescription and that training-induced
441 changes in individual lipid species and lipid classes are not stoichiometrically linked.

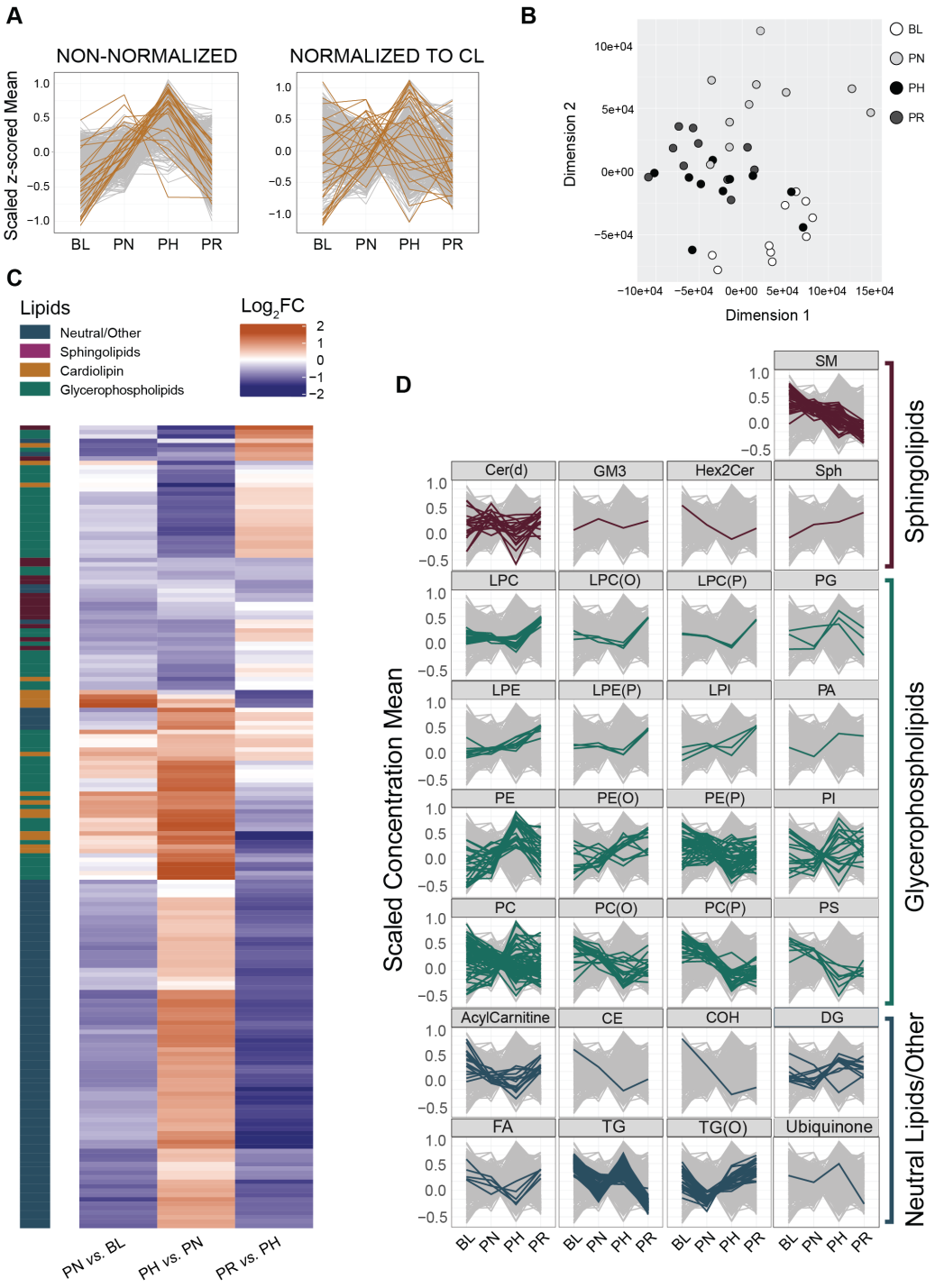

Figure 4. Lipidomics highlights a divergent response to training of different lipid classes

(A) All-lipids profile plot of non-normalized (left panel) and cardiolipin (CL) class-normalized (right panel) intensity values from mitochondrial isolates, displaying all individual CL species (gold) and all other lipid species (grey).

(B) Multidimensional scaling analysis showing segregation of samples obtained from IM fractions of lipidomics values normalized by the entire CL class.

449 (C) Heatmap of differentially expressed lipids after normalization by the entire CL class
450 between training phases determined with an adjusted $P < 0.05$ (Benjamini Hochberg). Row
451 clustering determined by unsupervised hierarchical cluster analysis.
452 (D) Profile plots of the scaled concentration mean of different lipid classes. For each profile
453 plot, all the individual lipid species identified within the specific class are represented in
454 color over the entire lipidome (grey) at each time point. The intensity values for all lipid
455 species were normalized by the entire CL class to adjust for changes in mitochondrial
456 content.
457 BL: baseline; PN: post-NVT; PH: post-HVT; PR: post-RVT. n = 10 for all analyses.

458 ***A training-induced increase in OXPHOS subunits is not a priority to enhance***
459 ***mitochondrial respiration.*** We next examined the OXPHOS pathway, which segregated
460 almost entirely in cluster-4 (Figure 2F and S2D; Table S5). Our analysis provided excellent
461 coverage of OXPHOS proteins and identified 78 OXPHOS subunits. We report training-
462 induced changes in 26 OXPHOS subunits (Figure 3), equivalent to 33% of all subunits
463 identified, most for the first time. Differentially expressed OXPHOS proteins included
464 subunits from all six of the modules required for the assembly of CI, both catalytic subunits
465 of CII, as well as subunits from CIII, one of the three core subunits of CIV, and proteins
466 found in both functional domains of CV. Specifically, we observed a large and coordinated
467 (23 subunits) decrease post-NVT, with no changes during HVT and/or RVT (Figure 3; Table
468 S7). Changes in SLC25A4 (ANT1), a protein catalyzing the exchange of cytosolic ADP and
469 mitochondrial ATP across the mitochondrial inner membrane (Palmieri, 2013), mirrored
470 these changes (Table S7). The post-NVT decrease in OXPHOS subunits indicates that during
471 times of increased mitochondrial biogenesis, synthesis of proteins involved in OXPHOS
472 pathways is deprioritized. Moreover, our results demonstrated a large post-NVT increase in
473 TCA cycle and FAO related enzymes - the major providers of reducing equivalents (NADH
474 and $FADH_2$) to the OXPHOS system (Wang and Hekimi, 2016); this suggests that
475 enhancement of these two metabolic pathways may be more important to improve

476 mitochondrial respiration following exercise training (Figure S1B, upper panels) than an
477 increase in OXPHOS subunits.

478 An increase in reducing equivalents coupled with the de-prioritization of the OXPHOS
479 machinery could lead to increased reactive oxygen species (ROS) generation. Here we report
480 an immediate post-NVT increase in the abundance of enzymes involved in protection from
481 oxidative stress, such as PRDX5 (the most increased protein), TXN2, and GPX1 (Powers et
482 al., 2020) (Figure 3; Table S7). Moreover, both SOD2, the mitochondrial ROS scavenger
483 (Powers et al., 2020), and PRDX5 were increased post-HVT and post-RVT. These findings
484 suggest that training-induced synthesis of proteins involved in the protection from oxidative
485 stress was emphasized early during the training intervention and maintained throughout,
486 consistent with the notion that exercise training provides protection against oxidative stress
487 (LaHue et al., 2016; Powers et al., 2020).

488 The coordinated assembly of OXPHOS complexes involves various assembly factors,
489 chaperones, and protein translocation components, and has been suggested to be in the order
490 of days (McKenzie et al., 2007). Whereas increases in OXPHOS assembly factors occurred
491 mostly post-HVT (Figure 3; Table S7), changes in subunits of the mitochondrial ribosome
492 (Figure 2C, lower right panel), which synthesize the 13 OXPHOS subunits encoded by
493 mitochondrial DNA, and in several chaperone proteins regulating import and folding of
494 proteins destined for the mitochondrial matrix, took place earlier (post-NVT; Figure 3; Table
495 S7). Chaperone proteins upregulated post-NVT included HSPA9 (mtHsp70), HSPD1
496 (mtHsp60), HSPE1 (mtHsp10), and TRAP1 (mtHsp75), whereby TIMM44 was increased
497 during HVT (Figure 3; Table S7). All five proteins remained elevated compared to BL both
498 post-HVT and post-RVT. Except for HSPE1 (Egan et al., 2011), none of the above
499 chaperones have previously been reported to respond to exercise. Owing to the notion that all

500 of these chaperones are known to interact (Voos, 2013), our data indicate a coordinated
501 increase in the protein quality control system in response to exercise training. While we
502 detected many subunits of the translocases of the outer and inner membrane (TOM and TIM,
503 respectively; Table S3), which are required for importing nuclear-encoded subunits
504 (Wiedemann and Pfanner, 2017), most did not change significantly with training, suggesting
505 that their levels remain stable relative to changes in mitochondrial content.

506 **Training-induced changes in mitochondrial content, but not changes in the abundance**
507 **and/or organization of SCs, mediate improvements in mitochondrial respiration**. A
508 previous study reported that training increases the formation of ETC SCs - high molecular
509 weight assemblies comprised of CI, CIII, and CIV (Schägger and Pfeiffer, 2000) - and
510 suggested this to contribute to improvements in mitochondrial respiration (Greggio et al.,
511 2017). Although SCs were originally proposed to support enhanced ETC function (Lapuente-
512 Brun et al., 2013), their role has become controversial, with multiple groups reporting that
513 they confer no bioenergetic advantage (Hirst, 2018). To provide further insight, we
514 performed BN-PAGE analysis of ETC SCs (Figure 5A). We observed increases in SC
515 abundance with increasing training volumes, achieving significance post-HVT (Figure 5B,
516 upper panels); however, these increases were no longer significant upon normalization by
517 MPE (Figure 5B, middle panels).

518 We next assessed whether exercise training affects the distribution of ETC complexes into
519 SCs. In contrast to the only previous report showing a post-training redistribution of CIII and
520 CIV (but not CI) into SCs in elderly individuals (Greggio et al., 2017), our analysis revealed
521 no significant changes throughout the intervention (Figure 5B, lower panels). This
522 demonstrates that in young healthy men, endurance training does not alter the ETC complex
523 distribution within major and minor SC assemblies. While the contrasting findings may relate

524 to differences in the participants' average age (66 *vs.* 22 y) and baseline $\dot{V}O_{2max}$ (1.9 *vs.* 3.6 L
525 min^{-1}), as well as the training interventions (48 sessions of moderate-intensity training in 16
526 weeks *vs.* 52 sessions of HIIT in 9 weeks), our results are consistent with the concept that SC
527 assemblies are a structural feature of the ETC rather than a phenomenon conferring enhanced
528 bioenergetics (Hirst, 2018). In line with this, our data indicated that the greatest changes in
529 maximal mitochondrial respiration ($[ETF+CI+II]_P$) occurred in parallel with the greatest
530 changes in SC abundance (compare Figure 5B with 5C, both upper panels). However,
531 following normalization by MPE, both of these adaptations were no longer significant
532 (compare Figure 5B, middle panels with Figure 5C, lower panel). Taken together, our
533 findings do not support the hypothesis that training-induced changes in the abundance or
534 organization of SCs contribute to improvements in mitochondrial respiration. Conversely, our
535 data indicate that training-induced changes in both mitochondrial respiration and SC
536 formation could largely be attributed to increases in mitochondrial content.

537 Given the importance of CLs for the assembly and stability of mitochondrial membrane
538 protein complexes and ETC SCs (Gebert et al., 2009; Pfeiffer et al., 2003), we again
539 interrogated our normalized mitochondrial lipidome. Our analysis demonstrated an extensive
540 remodeling of CL composition (Figure 5D); notably, following NVT and HVT, we observed
541 a decrease in the abundance of tetra-linoleoyl CL (18:2_18:2_18:2_18:2), the dominant form
542 of CLs found in skeletal muscle (Ikon and Ryan, 2017). Accompanying this were
543 concomitant increases in CLs containing oleic acid (18:1) and to a lesser extent palmitoleic
544 acid (16:1) acyl chains. This may reflect a lack in relative availability of dietary linoleic acid
545 due to increased mitochondrial biogenesis, since the nature of CL remodeling catalyzed by
546 TAZ, which was unaltered in our dataset, appears to be controlled predominantly by lipid
547 availability (Malhotra et al., 2009). This compensation in CL content is in line with our

548 observation that increased training volume does not lead to changes in ETC SC assembly

549 (Figure 5B middle and lower panels).

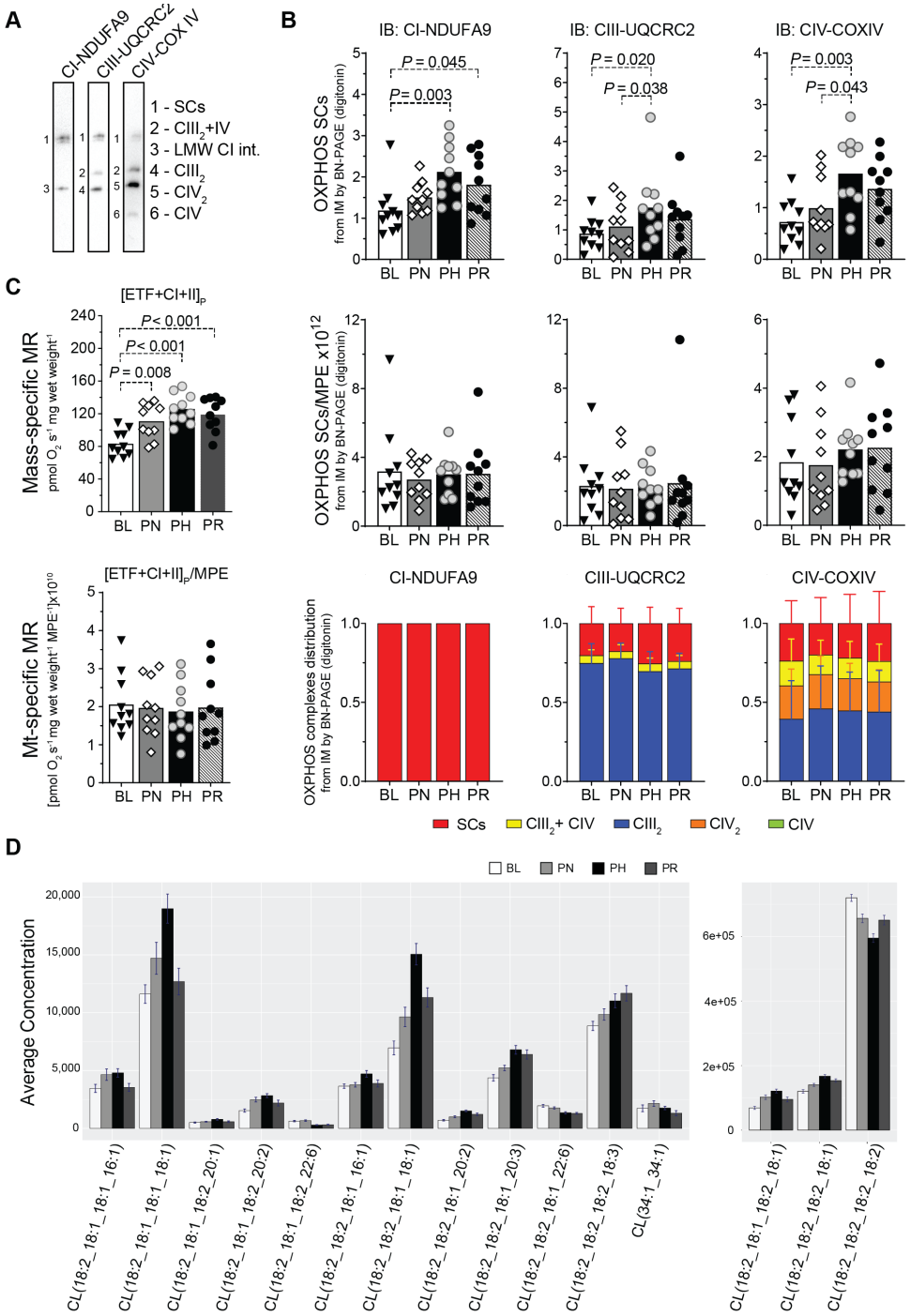

550

551 **Figure 5. Training-induced changes in mitochondrial content, but not changes in the**

552 **abundance and/or organization of SCs, mediate improvements in mitochondrial**

553 **respiration**

554 (A) Representative BN-PAGE blots of isolated mitochondria (IM) fractions from human

555 vastus lateralis muscles (images from baseline [BL] IM fractions). Band 1 (SCs): mature

556 supercomplexes (SCs) consisting of complex I+III_n+IV_n; band 2 ($CIII_2$+IV): a SC consisting
557 of CIII and CIV; band 3 (LMW CI int): low molecular weight intermediate of CI (band not
558 present in all samples); band 4 ($CIII_2$): CIII dimer; band 5 (CIV_2): CIV dimer; band 6 (CIV):
559 CIV monomer.
560 (B) Top panels: protein content of SCs of the electron transport chain (ETC) by BN-PAGE in
561 IM fractions from human vastus lateralis muscle biopsies (antibodies probed on separate
562 membranes); middle panels: values from top panels normalized by mitochondrial protein
563 enrichment (MPE); lower panels: distribution of ETC complexes into SCs from images
564 obtained in b at each time point.
565 (C) Top panel: maximal mass-specific mitochondrial respiration (MR) in permeabilized
566 human vastus lateralis muscle fibers with convergent electron input through ETF+CI+CII
567 ($[ETF+CI+II]_P$); lower panel: values of mitochondrial- (mt-) specific MR, obtained after
568 normalizing values from the top panel by MPE ($[ETF+CI+II]_P$/MPE). Results for the entire
569 substrate-uncoupler-inhibitor-titration (SUIT) protocol are shown in Figure S1B.
570 (D) Training-induced changes in all individual CL species that were differentially expressed
571 (as determined in Figure 4C, with an adjusted $P < 0.05$ [Benjamini Hochberg]).
572 PN: post-NVT; PH: post-HVT; PR: post-RVT; IB: immunoblotting. ▼,◊,○, and ● represent
573 individual values; bars represent mean values; error bars in c represent SD; n = 10 for all
574 analyses; datasets (B) and (C) were analyzed by repeated measures one-way ANOVA
575 followed by Tukey's post hoc testing, except for the lower right panel of (B), which was
576 analyzed by Friedman test followed by Dunn's post hoc testing, as not normally distributed.
577 Significance: $P < 0.05$.

578 ***Coenzyme Q biosynthesis and cristae formation are not prioritized during high-volume***
579 ***endurance training.*** Despite enrichment analysis suggesting cluster-5 to be enriched in
580 metabolism of amino acids and derivatives, upon further inspection we identified this cluster
581 to predominantly contain proteins involved in the biosynthesis and function of coenzyme Q
582 (CoQ or ubiquinone; Figure 2F and S2D; Table S5) - an enzyme with an essential role as an
583 electron transfer lipid in OXPHOS processes (Wang and Hekimi, 2019). We identified
584 changes in four constituents (COQ3, COQ5, COQ7, COQ9) of the CoQ synthome (Figure 3;
585 Table S6), a multi-subunit complex necessary for the biosynthesis of CoQ (Stefely and

586 Pagliarini, 2017). We report no changes post-NVT, consistent with previous research
587 investigating the effects of short-duration (< 3 weeks) exercise training on CoQ content in
588 human skeletal muscle (Svensson et al., 1999). However, post-HVT we report a concerted
589 reduction in three of these proteins, which also persisted post-RVT (Table S7). This indicates
590 that CoQ biosynthesis is not prioritized in response to high-volume endurance training,
591 suggesting that enhancing the CoQ pool may not be necessary to support an increase in
592 mitochondrial respiration in human skeletal muscle of young healthy individuals.

593 CoQ is an electron carrier shuttling electrons derived from the TCA cycle (via CI and CII),
594 pyrimidine biosynthesis (via DHODH), glycolysis (via GPD2), and FAO (via EFTDH) to
595 Complex III (Wang and Hekimi, 2016). Moreover, other enzymes located near or on the
596 inner mitochondrial membrane feeding electrons to CoQ, such as IVD (Finocchiaro et al.,
597 1987), DLD (Xia et al., 2001), and L2HGDH (Oldham et al., 2015), were also identified in
598 our study (Table S6). Similar to the decrease reported above in CI and CII subunits post-
599 NVT, we report decreases in four of these enzymes during HVT, with three of them
600 remaining downregulated both post-HVT and post-RVT; conversely, IVD was increased
601 during NVT and DHODH was elevated post-HVT (Figure 3; Table S7). The lack of a clear
602 correlation between the content of the above proteins and that of CoQ may be ascribed to
603 changing preferences for energy utilization over the course of the training intervention, as
604 also indicated by the differential prioritization of the various metabolic pathways described
605 above.

606 The mitochondrial contact site and cristae organizing system (MICOS) is pivotal for the
607 formation of cristae junctions, providing the extended membrane surface hosting OXPHOS
608 complexes (Huynen et al., 2016). The MICOS associates with the outer membrane sorting
609 and assembly machinery (SAM) to yield the mitochondrial intermembrane space bridging

610 complex (MIB), thus linking the mitochondrial inner and outer membranes (Huynen et al.,
611 2016). Eight proteins involved in cristae formation were differentially expressed in our study:
612 APOO (MIC26), APOOL (MIC27), CHCHD3 (MIC19), and MIC60 from the MICOS
613 complex; MTX1 and MTX2 from the SAM complex; TMEM11, a protein associating with
614 multiple MICOS subunits for cristae biogenesis (Guarani et al., 2015); and OMA1, a
615 mitochondrial protease regulating OPA1 (Ehses et al., 2009) - a key protein implicated in
616 cristae remodeling (Frezza et al., 2007) (Figure 3; Table S6). Seven of these proteins, which
617 almost entirely grouped within cluster-6 (Figure 2F and S2D; Table S5), were significantly
618 decreased post-HVT, with four being decreased post-RVT (Table S7). To our knowledge,
619 this is the first study to report a training-induced de-prioritization of these proteins. This is
620 consistent with the minimal changes observed in cristae density following short-term (< 3
621 months) exercise training in obese individuals (Nielsen et al., 2017). Thus, our results support
622 the notion that cristae remodeling is not a priority during short-term training and that changes
623 in other mitochondrial proteins are more important to adapt to the higher metabolic demand
624 of exercise. Despite MICOS-MIB subunits being known to interact with CLs (Weber et al.,
625 2013), we report no correlation between the levels of MICOS-MIB subunits and changes in
626 CLs content following different training volumes.

627 **CONCLUSION**

628 The present study utilized the power of a multi-omics approach, and a novel *in silico*
629 normalization strategy eliminating the bias introduced by changes in mitochondrial content,
630 to unearth an intricate and previously undemonstrated network of differentially prioritized
631 mitochondrial adaptations to exercise training in men. We identified 185 differentially
632 expressed mitochondrial proteins, an ~10-fold increase compared to previous studies. This
633 increased number of proteins was largely related to our normalization strategy, and does not
634 seem to depend on the large training volume utilized (120 differentially expressed proteins
635 would have been identified after the modest training volume of the NVT phase alone), nor is
636 the result of comparing multiple time points (118 differentially expressed proteins would
637 have been identified by sampling muscle only at the beginning and end of the study). This
638 increased depth of analysis enabled us to identify the time-dependent and complex
639 remodeling of the mitochondrial proteome following endurance exercise. We demonstrate
640 that training-induced changes in individual proteins, protein functional classes, and metabolic
641 pathways follow markedly different patterns of adaptation, which are not stoichiometrically
642 linked to the overall training-induced increase in mitochondrial content. Moreover, we show
643 that the lack of stoichiometry and the differential prioritization extended to all three levels
644 investigated (i.e., the transcriptome, proteome, and lipidome) and between levels, as
645 demonstrated by the delayed adaptive response of lipids compared to proteins.

646 A striking and unexpected finding was the early (post-NVT) deprioritization of OXPHOS
647 subunit formation, which indicates that the overall training-induced increase in biogenesis
648 and the proliferation of mitochondria is greater than the increase in specific components of
649 the OXPHOS machinery. This become even more striking when considering the early
650 increase in mitochondrial respiration, as well as proteins involved in the TCA cycle and FAO

651 processes - two of the main suppliers of reducing equivalents to the OXPHOS system. This
652 could not be explained by changes in the abundance and/or organization of SCs, as
653 previously hypothesized (Lapuente-Brun et al., 2013), as our findings showed no change in
654 these parameters, adding to the growing evidence that SC formation does not confer
655 enhancements in mitochondrial bioenergetics (Hirst, 2018). This is also unlikely to be related
656 to the lengthy time requirements necessary to assemble large multi-protein complexes
657 (McKenzie et al., 2007), as the relative amount of OXPHOS subunits remained reduced
658 throughout the intervention (lasting several weeks), whereas mitochondrial respiration, as
659 well as TCA cycle and FAO process, remained upregulated throughout. Instead, these
660 increases were likely supported by the inherent reserve capacity of mitochondria (i.e., their
661 ability to respond to sudden increases in energy requirements) (Desler et al., 2012), and
662 demonstrate that enhancing electron flow to OXPHOS is more important to increase ATP
663 production than an increase in the components of the OXPHOS machinery. The relative
664 decrease in proteins important for both CoQ biosynthesis and cristae formation further
665 substantiates these findings.

666 Finally, the above findings were the result of changes in only one of the several exercise
667 prescription programming variables (i.e., training volume). Future research should investigate
668 the effects of manipulating other programming variables (e.g., exercise intensity, frequency,
669 recovery between sessions), the type of exercise (e.g., running, swimming, resistance
670 training), and different populations (e.g., differences in age, sex, health status) utilizing a
671 similar approach. These interventions are likely to induce adaptations that are specific and
672 presumably different from the one presented here. Because of the well-documented
673 therapeutic benefits of exercise training (Booth et al., 2000; Pedersen and Saltin, 2006), the
674 knowledge generated by our novel findings, which are readily available in supplemental

675 tables, together with the results from future research, could be mined by exercise and health

676 professionals to design focused and personalized training interventions.

677 **Acknowledgments**. We thank the participants for their time and commitment to this study.
678 The authors would like to acknowledge all members of the Stroud and Bishop labs for input
679 into interpretation and presentation of data. We thank the Bio21 Mass Spectrometry and
680 Proteomics Facility (MMSPF) for provision of instrumentation, training, and technical
681 support. We acknowledge the use of the services and facilities of the Australian Genome
682 Research Facility (AGRF). This study was funded by grants from the ANZ-MASON
683 Foundation (to D.J.B), the Australian Research Council (Discovery Project DP140104165 to
684 D.J.B), the Australian National Health and Medical Research Council (NHMRC Project
685 Grant 1140906 to D.A.S.; NHMRC Fellowships 1140851 to D.A.S. and 1155244 to D.R.T.),
686 JDRF Australia (JDRF Career Development to M.T.C.), and the Australian Research Council
687 Special Research Initiative in Type 1 Juvenile Diabetes (to M.T.C.). We acknowledge the
688 support of the Mito Foundation for the provision of instrumentation and the Victorian
689 Government's Operational Infrastructure Support Program.

690 **Author contributions.** C.G., D.A.S., and D.J.B. conceptualized the study. C.G., D.A.S., and
691 D.J.B. devised the study methodology. C.G., N.A.J., and H.A.J. performed study validation.
692 C.G., N.A.J, H.A.J. delivered the training and performed sample collection. C.G., J.B., J.K.,
693 B.R., A.L., T.L.S., and A.E.F. performed biochemical analyses. C.G., B.R., and D.A.S.,
694 performed proteomic analysis. K.H., and N.A.M. performed lipidomic analysis. RNA-seq
695 analysis was performed at the Australian Genome Research Facility (AGRF). C.G., N.J.C.,
696 and D.A.S. performed statistical and bioinformatic analysis. C.G., N.J.C., and D.A.S.
697 delivered the visualization. C.G., D.A.S., and D.J.B. wrote the manuscript. M.T.C., P.J.M.,
698 D.R.T., D.A.S, and D.J.B. provided supervision. D.R.T., M.T.C., D.A.S, and D.J.B. funded
699 the research. C.G., D.A.S., and D.J.B. have primary responsibility for final content. Data
700 collection took place at Victoria University. Muscle analysis took place at Victoria
701 University, Monash University, Murdoch Children's Research Institute, the Baker Heart &

Diabetes Institute, AGRF, and the Bio21 Molecular Science & Biotechnology Institute (The University of Melbourne). All persons designated as authors qualify for authorship, and all those qualifying for authorship are listed. All authors have read and approved the final manuscript.

Declaration of interests. The authors declare no conflict of interest.

707 **STAR METHODS**

708 **RESOURCE AVAILABILITY**

709 **Lead Contact and Materials Availability.** Further information and requests for resources
710 and reagents should be directed to and will be fulfilled by the lead contacts, David Stroud
711 (david.stroud@unimelb.edu.au) and David Bishop (david.bishop@vu.edu.au). This study did
712 not generate new unique reagents.

713 **Data and Code Availability.** The mass spectrometry proteomics data will be deposited to the
714 ProteomeXchange Consortium via the PRIDE partner repository upon publication. The
715 transcriptomic data will be deposited to NCBI upon publication. Lipidomics data will be
716 deposited to the Metabolomics Workbench Data Repository. The R scripts used for all omics
717 analyses described above are deposited on GitHub at
718 https://github.com/XercisOmics/EnduranceMitoMultiOmics.

719 **EXPERIMENTAL MODEL AND SUBJECT DETAILS**

720 Ten healthy men volunteered to take part in this study (physiological and performance
721 parameters are presented in Table 1). Potential participants were deemed suitable if aged 18-
722 35 y, were moderately-trained (i.e., less than 4 h per week of unstructured aerobic activity for
723 half a year prior to the study), not regularly engaged in cycling-based sports, and were non-
724 smokers and medication free prior to and during the study. Participants underwent a medical
725 screening to exclude conditions that may have precluded their participation (e.g.,
726 cardiovascular, musculoskeletal and/or metabolic problems), and were informed of the study
727 requirements, risks, and benefits, before giving written informed consent. Approval for the
728 study's procedures, which conformed to the standards set by the latest revision of the

729 Declaration of Helsinki, was granted by the Victoria University Human Research Ethics
730 Committee (HRE15-126).

731 **METHOD DETAILS**

732 ***Study design.*** The study consisted of three consecutive training phases: the normal- (NVT),
733 high- (HVT), and reduced- (RVT) training volume phase (Figure 1A). Each training phase
734 was preceded (and followed) by performance testing, which included a 20-km cycling time
735 trial (20k-TT), a graded exercise test (GXT) (participants were previously familiarized with
736 both tests), and a resting muscle biopsy. Overall study duration was ~9 weeks.

737 ***Testing procedures.*** Participants were required to avoid any vigorous exercise for the 48 h
738 preceding each performance test (72 h for the skeletal muscle biopsy), from alcohol and any
739 exercise for 24 h before testing, and from food and caffeine consumption for the 2 h
740 preceding each test. Similar tests were performed at the same time of the day throughout the
741 study to avoid variations caused by changes in circadian rhythm.

742 *GXT.* A graded exercise test was performed on an electronically-braked cycle ergometer
743 (Lode Excalibur v2.0, Groningen, The Netherlands) to determine peak oxygen uptake
744 ($\dot{V}O_{2Peak}$), peak power output ($\dot{W}_{Peak}$), the power attained at the lactate threshold ($\dot{W}_{LT}$) using
745 the modified D_{Max} method (Bishop et al., 2000), and the training intensity for each training
746 phase. The test consisted of consecutive 4-min stages at constant power output; the test
747 starting intensity (range: 45-77 W) and the intensity increase of each stage (range: 17-28 W)
748 were chosen so as to obtain at least 8 time points for the determination of the $\dot{W}_{LT}$ (Jamnick et
749 al., 2018) and were based on participants' fitness levels. An identical protocol was used at all
750 4 time points for each participant. Prior to the test, and in the last 30 s of each stage, venous
751 blood samples were taken for measurement of blood lactate concentration ($[La^-]$). Participants

752 were instructed to keep a cadence > 60 rpm and were only allowed access to cadence. The
753 test was stopped when a participant reached volitional exhaustion or cadence dropped below
754 60 rpm for over 10 s. The $\dot{W}_{Peak}$ was determined as the power of the last completed stage plus
755 an additional 25% of the stage increase wattage for every additional minute completed. At the
756 end of each GXT, after a 5-min recovery, a verification exhaustive bout was performed at an
757 intensity equivalent to $\dot{V}O_{2Peak}$ to confirm the highest measured $\dot{V}O_{2Peak}$ (Jamnick et al.,
758 2018).

759 *20k-TT.* Cycling time trials were performed on an electronically-braked cycle ergometer
760 (Velotron, RacerMate, Seattle, WA, USA) after a 6-min cycling warm-up (4 min at 66% of
761 $\dot{W}_{LT}$ followed by 2 min at $\dot{W}_{LT}$), and 2 min of rest. Participants were only allowed access to
762 cadence and completed distance.

763 *Gas Analysis during the GXT.* During the GXT, expired air was continuously analyzed for O_2
764 and CO_2 concentrations via a gas analyzer (Moxus 2010, AEI Technologies, Pittsburgh, PA,
765 USA), which was calibrated immediately before each test. $\dot{V}O_2$ values were recorded every
766 15 s and the average of the two highest consecutive 15-s values was recorded as a
767 participant's $\dot{V}O_{2Peak}$.

768 *Venous blood sampling.* Venous blood samples (~1 mL) were collected during the GXT from
769 a cannula inserted in the antecubital vain for the determination of venous blood [La^-] using a
770 blood-lactate analyzer (2300 STAT Plus; YSI, Yellow Spring, OH, USA).

771 *Muscle biopsies.* A biopsy needle with suction under local anesthesia (1% xylocaine) was
772 used to obtain vastus lateralis muscle biopsies at rest at the following four time points: BL,
773 PN, PH and PR. After being cleaned of excess blood, connective and fat tissue muscle
774 biopsies were divided as follows: ~10 mg was immediately immersed in ~2 mL of ice-cold

775 BIOPS for measurements of mitochondrial respiration, whereas the remainder was promptly
776 frozen in liquid nitrogen and stored at -80°C for follow-up analyses.

777 ***Training intervention.*** All training sessions were performed on an electronically braked
778 cycle ergometer (Velotron, RacerMate, USA), following an 8-min warm up (see 20k-TT) and
779 consisted of HIIT (2:1 work-to-rest ratio). Training intensity was set relative to $\dot{W}_{LT}$ (rather
780 than $\dot{W}_{Peak}$) so as to induce similar metabolic and cardiac stresses amongst participants of
781 differing fitness levels (Baldwin et al., 2000). Exercise intensity was maintained between
782 $\dot{W}_{LT}$ and $\dot{W}_{Peak}$ throughout the entire study so that training volume was the only manipulated
783 variable between the 3 phases.

784 *NVT phase.* This consisted of 6 HIIT sessions within 2 weeks of 5 to 7 4-min cycling
785 intervals interspersed with a 2-min recovery at 60 W. Exercise intensities were defined as
786 $[\dot{W}_{LT} + x(\dot{W}_{Peak}-\dot{W}_{LT})]$, with x increasing from 0.5 to 0.7 throughout the phase.

787 *HVT phase.* Participants performed HIIT twice a day for 20 consecutive days; training
788 sessions consisted of either 7 to 10 4-min intervals interspersed with a 2-min recovery at 60
789 W at intensities ranging from $[\dot{W}_{LT} + 0.5(\dot{W}_{Peak}-\dot{W}_{LT})]$ to $[\dot{W}_{LT} + 0.8(\dot{W}_{Peak}-\dot{W}_{LT})]$, or 15 to 20
790 2-min intervals at intensities ranging from $[\dot{W}_{LT} + 0.5(\dot{W}_{Peak}-\dot{W}_{LT})]$ to $[\dot{W}_{LT} + 0.95(\dot{W}_{Peak}-$
791 $\dot{W}_{LT})]$, interspersed with a 1-min recovery at 60 W. Single session duration increased from
792 ~45 min to 60 min.

793 *RVT phase.* The RVT phase consisted of 6 HIIT sessions in 6 days; participants performed
794 10, 9, 8, 7, 6, and 4, 4-min intervals interspersed with a 2-min recovery at 60 W, at an
795 intensity of $[\dot{W}_{LT} + x(\dot{W}_{Peak}- \dot{W}_{LT})]$, with x increasing from 0.5 to 0.7 throughout the phase.

796 ***Physical activity and nutritional control.*** Physical activity and dietary patterns were
797 maintained throughout the study and were monitored with the use of food and physical
798 activity recall diaries. The last 3 meals prior to each performance test undertaken during
799 baseline testing were recorded by each participant and were replicated thereafter before the
800 same type of test. To control for dietary effects on muscle metabolism, participants were
801 provided with a standardized dinner (55 kJ kg^{-1} body mass (BM), providing 2.1 g
802 carbohydrate (CHO) kg^{-1} BM, 0.3 g fat kg^{-1} BM, and 0.6 g protein kg^{-1} BM) and breakfast
803 (41 kJ kg^{-1} BM, providing 1.8 g CHO kg^{-1} BM, 0.2 g fat kg^{-1} BM, and 0.3 g protein kg^{-1} BM),
804 to be consumed 15 and 3 h prior to the muscle biopsy, respectively.

805 ***Muscle analyses***

806 *Enzymatic activity.* Enzyme activities were determined spectrophotometrically in post-600g
807 supernatants of skeletal muscle homogenates according to the method described for
808 respiratory chain complexes I-IV and citrate synthase (Frazier et al., 2020). Briefly, ~20mg of
809 skeletal muscle sample was homogenized in sucrose/mannitol containing buffer using a
810 glass/glass homogenizer and spun for 10 min at 600 g and 4 °C. The supernatant was then
811 subjected to two freeze/thaw cycles and stored at -80 °C until measurement of respiratory
812 chain enzymes. CI was assayed as rotenone-sensitive NADH:CoQ1 oxidoreductase by
813 monitoring the decrease in absorbance due to NADH oxidation at 340 nm. For CII, activity
814 was measured as succinate:CoQ1 oxidoreductase by measuring CoQ1 reduction at 280 nm.
815 CIII was assayed as decylbenzylquinol; cytochrome *c* oxidoreductase by following the
816 increase in absorbance resulting from cytochrome *c* reduction at 550 nm. CIV was measured
817 as cytochrome *c* oxidase by following the decrease in absorbance resulting from cytochrome
818 *c* oxidation at 550 nm. To assay the CS catalyzed production of coenzyme A (CoA.SH) from
819 oxaloacetate, the generation of free sulfhydryl groups was monitored using the thiol reagent

820 5,5'-dithio-bis-(2-nitobenzoic acid) (DTNB), which reacts spontaneously with the sulfhydryl
821 groups to produce 5-thio-2-nitrobenzoate anions. CS specific activity was measured by
822 following the increase in absorbance resulting from the formation of 5-thio-2 nitrobenzoate
823 anions at 412nm. Following the enzyme measurements, the amount of protein in each sample
824 was determined using a bicinchoninic acid assay and activity calculated as initial rates
825 (complexes I, II and citrate synthase) or as first-order rate constants (complexes III and IV).

826 *Preparation of whole-muscle lysates for SDS-PAGE assessment of ETC subunits.* Frozen
827 skeletal muscle samples (~10 mg) were homogenized in a TissueLyser for 2x 2 min at
828 maximum speed in ice-cold lysis buffer (1:20 w/v) containing 50 mM Tris-HCl, 150 mM
829 NaCl, 1 mM EDTA, 1% NP-40 and a phosphatase/protease inhibitor (5872, Cell Signaling
830 Technology, Danvers, MA, USA). Homogenates were rotated end-over-end at 4 °C for 1 h
831 and protein concentration was determined in triplicate using a commercial colorimetric assay
832 (Bio-Rad Protein Assay kit-II, Australia).

833 *Mitochondrial isolation for SDS- and BN-PAGE assessment of ETC subunits, complexes and*
834 *SCs*. Frozen skeletal muscle samples (~30 mg) were homogenized with 2x 20 strokes in a
835 Potter-Elvehjem tissue grinder attached to a rotating drill (~1000 rpm) in 5 mL solution A (1
836 mM EDTA, 220 mM mannitol, 20 mM HEPES-KOH [pH=7.6], 70 mM sucrose, 2 mg/mL
837 BSA, 0.5 mM PMSF) and spun at 800 g for 5 min at 4°C. The supernatant was collected,
838 whereas the pellet was re-homogenized as above in 5 mL of solution A to maximize
839 extraction. The two supernatants were mixed and further spun at 800 g for 5 min at 4°C. The
840 ensuing supernatant was then spun at 10,000 g for 20 min at 4°C, and the pellet was
841 resuspended in 200 µL of sucrose buffer (0.5 M sucrose, 10 mM HEPES-KOH [pH=7.6], 0.5
842 mM PMSF). Protein concentration was determined by the bicinchoninic acid method
843 according to the manufacturer's instructions (BCA Protein Assay Kit, Pierce-Thermo Fisher

844 Scientific, Melbourne, Australia). This measurement was used to generate Figure 1C.

845 *SDS-PAGE.* Both whole-muscle lysates (7.5 µg) and mitochondrial isolates (5 µg) were
846 separated by electrophoresis using 12 or 15% SDS-PAGE gels, as previously described
847 (Granata et al., 2016b), and blotted with a total OXPHOS (ab110411, Abcam, Cambridge,
848 MA, USA) or with a single CI (ab110242, Abcam, Cambridge, MA, USA) antibody where
849 separation with CIV was not optimal using the total OXPHOS antibody.

850 *BN-PAGE.* Mitochondrial isolates (6-15 µg) were separated by electrophoresis using 3-12%
851 NativePAGE gels (Life Technologies Australia, Mulgrave, Australia) as previously described
852 (Jha et al., 2016). A 4 g/g digitonin/protein ratio was used for assessment of SCs. The
853 following primary antibodies were used: NADH:ubiquinone oxidoreductase subunit A9
854 (NDUFA9; ab14713), ubiquinol-cytochrome *c* reductase core protein 2 (UQCRC2; ab14745),
855 cytochrome *c* oxidase subunit IV (COX IV; ab14744) (all Abcam, Cambridge, MA, USA).

856 For both SDS- and BN-PAGE, protein bands were visualized using a Bio-Rad ChemiDoc
857 imaging system and bands were quantified using Bio-Rad Image Lab 5.0 software (Bio-Rad
858 laboratories, Gladesville, NSW, Australia). An internal standard (made of a mixture of all
859 samples) was loaded in each SDS- and BN-PAGE gel, and each lane was normalized to this
860 value, to reduce gel-to-gel variability.

861 *Fiber preparation for high-resolution respirometry.* Fresh muscle fibers were mechanically
862 separated in ice-cold BIOPS (in mM: 2.77 CaK_2EGTA, 7.23 K_2EGTA, 5.77 Na_2ATP, 6.56
863 $MgCl_2$, 20 taurine, 50 MES, 15 Na_2phosphocreatine, 20 imidazole and 0.5 dithiothreitol
864 adjusted to pH 7.1 (Pesta and Gnaiger, 2012), followed by permeabilization by gentle
865 agitation for 30 min at 4°C in BIOPS containing 50 µg/mL of saponin, and 3 5-min washes in
866 MiR05 (in mM, unless specified: 0.5 EGTA, 3 $MgCl_2$, 60 K-lactobionate, 20 taurine, 10

867 KH_2PO_4, 20 HEPES, 110 sucrose and 1 g/L BSA essentially fatty acid-free, pH 7.1) (Pesta
868 and Gnaiger, 2012). Mitochondrial respiration was measured in duplicate (from 2-3 mg wet
869 weight of muscle fibers) in MiR05 at 37°C using the high-resolution Oxygraph-2k (Oroboros,
870 Innsbruck, Austria). To avoid potential oxygen diffusion limitation, oxygen concentration
871 was maintained between 270 and 480 nmol mL^{-1} by re-oxygenation via direct syringe
872 injection of O_2.

873 *Mitochondrial respiration protocol.* The substrate-uncoupler-inhibitor titration (SUIT)
874 protocol (Pesta and Gnaiger, 2012) used was as follows: 0.2 mM octanoylcarnitine and 2 mM
875 malate ($[ETF]_L$: leak respiration state [L] in the absence of adenylates and limitation of flux
876 by electron input through electron transfer flavoprotein [ETF]); 3 mM $MgCl_2$ and 5 mM ADP
877 ($[ETF]_P$: maximal OXPHOS capacity [P] with saturating levels of ADP and limitation of flux
878 by electron input through ETF); 5 mM pyruvate ($[ETF+CI]_P$: P with saturating levels of ADP
879 and limitation of flux by convergent electron input through ETF + CI); 10 mM succinate
880 ($[ETF+CI+II]_P$: P with saturating levels of ADP and limitation of flux by convergent electron
881 input through ETF + CI + CII); 10 µM cytochrome *c* (outer mitochondrial membrane
882 integrity test); 0.75-1.5 µM carbonyl cyanide 4-(trifluoromethoxy) phenylhydrazone (FCCP)
883 via stepwise titration ($[ETF+C+II]_E$, maximal electron transport chain capacity [E] with
884 saturating levels of ADP and limitation of flux by convergent electron input through ETF +
885 CI + CII); 0.5 µM rotenone ($[CII]_E$: E with saturating levels of ADP and limitation of flux by
886 electron input through CII); 5 µM antimycin A (residual non-mitochondrial oxygen
887 consumption [ROX]). Data are presented as mass-specific mitochondrial respiration [pmol O_2
888 s^{-1} mg^{-1} wet weight] and as mitochondrial-specific respiration [pmol O_2 s^{-1} mg^{-1} wet
889 weight/CS activity].

890 *RNA-seq analysis.* Approximately 10 to 15 mg of frozen muscle was used to isolate RNA

891 using the RNeasy Mini Kit (Qiagen, Canada) according to the manufacturer's instructions.
892 Samples were homogenized using the TissueLyser II (Qiagen, Canada). RNA concentration
893 and purity were determined spectrophotometrically (NanoDrop 2000, Thermo Fisher
894 Scientific, Wilmington, DE, USA) at 260 and 280 nm. RNA integrity was assessed using an
895 Agilent Bioanalyzer according to manufacturer's instructions. The RNA was stored at -80 °C.

896 *Sequencing and assembly of RNA-seq*. This analysis was conducted on n = 5 participants (20
897 samples in total); samples were sequenced (100 base pair, single reads) on the Illumina
898 NovaSeq 6000 platform at the Australian Genome Research Facility (AGRF). Transcriptome
899 assembly was completed at AGRF with reads screened for presence of any Illumina
900 adapter/overrepresented sequences and cross-species contamination. Per base sequence
901 quality for all samples was >96% bases above Q30. Cleaned sequence reads were aligned
902 against the *Homo sapiens* genome (Build version HG38). The STAR aligner (v2.5.3a) was
903 used to map reads to the genomic sequences. Count of read mapping to each known gene
904 were summarized to provide the matrix used for further analysis.

905 *Bioinformatic analysis of RNA-seq data.* For downstream RNA-seq analysis the R package
906 *limma* (Ritchie et al., 2015) was used to conduct the differential expression analysis from
907 count data. Count data was normalized using calcNormFactors in the *edgeR* package in R.
908 Differential expression analysis was performed between each subsequent biopsy to show
909 comparative changes between each of the training volumes, though all comparisons were
910 accounted for within the analysis. The resulting differential expression values were filtered
911 for an adjusted P value < 0.05 using the Benjamini Hochberg method. Heatmaps were
912 visualized using hierarchical clustering using the "average" method. Categorical columns for
913 the generation of Figure 1F were determined by identifying the transcripts to known
914 descriptions in the literature; MICOS (Eramo et al., 2020), TCA cycle (Martínez-Reyes and

915 Chandel, 2020), SLC25A (Palmieri, 2013), Assembly Factors (Hock et al., 2020). All
916 differentially expressed transcripts were run through Enrichr
917 [https://maayanlab.cloud/Enrichr/ (Chen et al., 2013; Kuleshov et al., 2016)] and the top
918 biological processes were identified with a combined score sorting for Figure 1G.

919 *Mitochondrial isolation for proteomics and lipidomics assessment.* Frozen skeletal muscle
920 samples (~30 mg) were homogenized with 2x 20 strokes in a Potter-Elvehjem tissue grinder
921 attached to a rotating drill (~1000 rpm) in 3 mL solution B (1 mM EDTA, 220 mM mannitol,
922 20 mM HEPES-KOH [pH=7.6], 70 mM sucrose, 0.5 mM PMSF) and spun at 1000 g for 5
923 min at 4°C. The supernatant was further spun at 12000 g for 10 min at 4°C, and the ensuing
924 pellet was resuspended in 200 µL of sucrose buffer (0.5 M sucrose, 10 mM HEPES-KOH
925 [pH=7.6]). Protein concentration was determined by the bicinchoninic acid method according
926 to the manufacturer's instructions (BCA Protein Assay Kit, Pierce-Thermo Fisher Scientific,
927 Melbourne, Australia). Two IM fractions per sample (50 µg each) were spun at 12000 g for
928 10 min at 4°C; after removal of the supernatant, the pellets were stored frozen at -80°C for
929 subsequent proteomics and lipidomics analysis.

930 *Proteomics.* IM fractions were prepared for proteomics analysis as previously described
931 (Stroud et al., 2016) with minor modifications. Briefly, 50 µg of frozen mitochondrial isolates
932 were solubilized in 20 µL of 8 M urea, 40 mM chloroacetamide, 10 mM tris(2-
933 carboxyethyl)phosphine, 100 mM Tris, pH 8.1; this was followed by 15 min of sonication in
934 a water bath sonicator and 30 min of shaking (1500 rpm, at 37°C). The urea concentration
935 was reduced to 2 M with H_2O prior to protein digestion with trypsin (Promega, Alexandria,
936 NSW, Australia) at a 1:60 trypsin:protein ratio and subsequent overnight digestion at 37°C.
937 The next day, samples were acidified with trifluoroacetic acid (1% [v/v] final concentration)
938 and centrifuged for 5 min at 20,100 g at RT. The supernatants were desalted on pre-activated

939 (100% acetonitrile [ACN]) and pre-equilibrated (0.1% TFA, 2% ACN) Empore™ SPE Disks
940 (matrix active group polystyrene-divinylbenzene [SDB-XC] Merck, Bayswater, VIC,
941 Australia) stage tips (Kulak et al., 2014) made in-house, before being washed (0.1% TFA, 2%
942 ACN) and eluted in 0.1% TFA, 80% ACN. Samples were concentrated under vacuum and
943 reconstituted in 0.1% TFA, 2% ACN. After 15 min sonication and subsequent vortexing
944 samples were centrifuged at 20,100 g at RT before estimation of peptide concentration
945 (Direct Detect, Merck). Approximately 600-800 ng of peptides were analyzed on a Thermo Q
946 Exactive™ Plus mass spectrometer coupled to an Ultimate 3000 HPLC (both Thermo Fisher
947 Scientific, Mulgrave, VIC, Australia). Peptides were first loaded onto a trap column (Dionex-
948 C18, 100 Å, 75 µm x 2 cm; Thermo Fisher Scientific) at an isocratic flow of 5 µL min^{-1} of
949 2% (v/v) ACN containing 0.1 % (v/v) formic acid (FA) for 5 min before switching the trap-
950 column in line with the analytical column (Dionex-C18, 100 Å, 75 µm x 50 cm; Thermo
951 Fisher Scientific). The separation of peptides was performed at 300 nL min^{-1} using a
952 nonlinear ACN gradient of buffer A (2% ACN, 0.1% FA) and buffer B (80% ACN, 0.1%
953 FA) over 125 min including void and equilibration. Data were collected in positive mode
954 using Data Dependent Acquisition using m/z 375–1400 as MS scan range, HCD for MS/MS
955 of the 15 most intense ions with $z \geq 2$. Other instrument parameters were: MS1 scan at 70,000
956 resolution (at 200 m/z), MS maximum injection time 50 ms, AGC target 3e6, stepped
957 normalized collision energy of 27, 30, 32, isolation window of 1.6 m/z, MS/MS resolution
958 17,500, MS/MS AGC target of 5e4, MS/MS maximum injection time 50 ms, minimum
959 intensity was set at 2e3 and dynamic exclusion was set to 30 s.

960 Raw files were analyzed using the MaxQuant platform (Cox and Mann, 2008) version
961 1.6.1.0, searching against the Uniprot human database containing reviewed, canonical
962 variants in FASTA format (June 2018) and a database containing common contaminants by
963 the Andromeda search engine (Cox et al., 2011). Default search parameters for a label free

964 quantification (LFQ) experiment were used with modifications. In brief, "Label free
965 quantification" was set to "LFQ" using a minimum ratio count of 2. Cysteine
966 carbamidomethylation was used as a fixed modification, and N-terminal acetylation and
967 methionine oxidation were used as variable modifications. False discovery rates of 1% for
968 proteins and peptides were applied by searching a reverse database, and 'match from and to',
969 'match between runs' options were enabled with a match time window of 0.7 min. Unique
970 and razor peptides with a minimum ratio count of 2 were used for quantification.

971 *Bioinformatic analysis of proteomics data.* The R package *limma* (Ritchie et al., 2015) was
972 used to conduct the differential expression analysis of MaxQuant LFQ intensities (extracted
973 from proteinGroups.txt) after first performing normalization using variance stabilizing
974 normalization (VSN) as found in the *limma* package. Identifications labelled by MaxQuant as
975 'only identified by site', 'reverse' and 'potential contaminant' were removed. Proteins having
976 less than 70% valid values were removed and remaining missing data was imputed using
977 QRILC method from the *imputeLCMD* package in R (Lazar). Differential expression
978 analysis was performed between BL and then each subsequent time point to show
979 comparative changes between each of the training volumes, though all comparisons were
980 accounted for within the analysis. Linear modelling was determined using eBayes in the
981 *limma* package. The resulting differential expression values were filtered for an adjusted *P*
982 value < 0.01 using the Benjamini Hochberg method. For the mitochondrial normalization, all
983 "Known Mitochondrial" proteins identified using the Integrated Mitochondrial Protein Index
984 (IMPI) (Smith and Robinson, 2019) were subset from the rest of the dataset, and then
985 followed the normalization and statistical validation as described above. Heatmaps were
986 produced using hierarchical clustering using the "complete" method. Gene ontology of the
987 clusters was determined by taking the proteins identified in the cluster and performing an
988 enrichment analysis using the ClueGO (v2.5.6) application in Cytoscape (v3.7.1) using

989 default settings except for a GO tree interval of 3 to 5, with only the Biological Processes
990 Ontology switched on (Figure 2F and Figure S2A). Full tables of identified proteins and post-
991 normalization differentially expressed proteins in their respective clusters and their
992 annotations can be found in Table S3 to 7.

993 The heatmaps presented in Figure 3 and discussed in the Results section were generated
994 according to Reactome pathways and/or literature searches (Table S6). Proteins involved in
995 two or more pathways were either presented in both pathways, or were assigned to the
996 pathway involving the protein's primary function and/or most closely matching their training-
997 induced changes. Specifically, "mitochondrial translation" was based on Reactome pathway
998 R-HSA:5368287 (Mitochondrial translation). "TCA cycle" was based on Reactome pathway
999 "R-HSA:71403 (Citric acid cycle [TCA cycle]); NNT was removed because its main
1000 physiological function is the generation of NADPH (Kampjut and Sazanov, 2019). "FAO"
1001 was based on Reactome pathway R-HSA:556833 (Metabolism of Lipids); ETFA (Watmough
1002 and Frerman, 2010), ETFB (Watmough and Frerman, 2010), HSD17B10 (Schulz, 1991), and
1003 PLIN5 (Benador et al., 2019) were added based on their involvement with FAO and lipid
1004 metabolism; GPD2 (Mráček et al., 2013; Wang and Hekimi, 2016), GPX1 [R-HSA-3299685
1005 and (Powers et al., 2020)], and GPX4 (Powers et al., 2020) where not presented within this
1006 pathway as their primary function suggested their inclusion in different pathways of Figure 3;
1007 SAR1B was removed because its main function is the regulation of vesicle budding (Takai et
1008 al., 2001). "OXPHOS" was based on Reactome pathway R-HSA:1632000 (Respiratory
1009 electron transport, ATP synthesis by chemiosmotic coupling, and heat production by
1010 uncoupling proteins); ETFA (Watmough and Frerman, 2010), ETFB (Watmough and
1011 Frerman, 2010), ETFDH (Wang and Hekimi, 2016), TRAP1 (Voos, 2013), and CYCS (R-
1012 HSA-3299685) were not presented within this pathway as their primary function and/or
1013 training-induced changes suggested their inclusion in different pathways of Figure 3 was

1014 more appropriate; based on the main function of its constituent proteins the “OXPHOS”
1015 pathway was then subdivided in 2 subgroups: “OXPHOS - subunits”, to which MP68
1016 (Fujikawa et al., 2014) was added, and “OXPHOS - Assembly factors” to which ATPAF1
1017 (Signes and Fernandez-Vizarra, 2018), BCS1L (Signes and Fernandez-Vizarra, 2018), and
1018 COA3 (Signes and Fernandez-Vizarra, 2018) were added. “Response to ROS” was based on
1019 Reactome pathway: R-HSA-3299685 (Detoxification of Reactive Oxygen Species); GPX4
1020 was added based on its ability to reduce H_2O_2 (Powers et al., 2020). “Protein Folding” was
1021 based on literature searches: TRAP1, HSPA9, HSPD1, HSPE1, and TIMM44 were all added
1022 based on their involvement in protein folding and quality control mechanisms (Voos, 2013).
1023 "CoQ biosynthesis" was based on Reactome pathway R-HSA-2142789 (Ubiquinol
1024 biosynthesis). “CoQ e- donors” was based on literature searches: DHODH (Wang and
1025 Hekimi, 2016), ETFDH (Wang and Hekimi, 2016), GPD2 (Wang and Hekimi, 2016), IVD
1026 (Finocchiaro et al., 1987), DLD (Xia et al., 2001) and L2HGDH (Oldham et al., 2015), were
1027 all added based on their function to feed electrons into the respiratory chain via CoQ. "Cristae
1028 formation" was based on Reactome pathway R-HSA-8949613 (Cristae formation); OMA1
1029 (Ehses et al., 2009; Frezza et al., 2007) was added based on its involvement in cristae
1030 formation, whereas ATP5A1, ATP5J, ATP5B, ATP5H, and ATP5O (all based on R-
1031 HSA:163200), as well as HSPA9 (Voos, 2013) were not presented within this pathway as
1032 their primary function suggested their inclusion in different pathways of Figure 3.

1033 *Lipid extraction for lipidomics.* Mitochondrial isolates were extracted using a modified
1034 single-phase chloroform/methanol extraction as described previously (Weir et al., 2013). In
1035 brief, 20 volumes of chloroform:methanol (2:1) were added to the sample along with a series
1036 of internal standards. Samples were vortexed and centrifuged on a rotary mixer for 10 min.
1037 Following sonication on a sonicator bath for 30 min, samples were rested for 20 min prior to
1038 centrifugation at 13,000 g for 10 min. Supernatants were transferred into a 96 well plated,

1039 dried down and reconstituted in 50 μL H_2O saturated butanol and sonicated for 10 min. After
1040 the addition of 50 μL of methanol with 10 mM ammonium formate, samples were
1041 centrifuged at 4000 rpm on a plate centrifuge and transferred into glass vials with inserts for
1042 mass spectrometry analysis.

1043 *Targeted lipidomics analysis.* LC-MS/MS was performed according to previously published
1044 methods, with slight modification for tissue samples (Huynh et al., 2019). Sample extracts
1045 were analyzed using either (i) an AB Sciex Qtrap 4000 mass spectrometer coupled to an
1046 Agilent 1200 HPLC system for CL assessment, as described preciously (Tan et al., 2020) or
1047 (ii) an Agilent 6490 QQQ mass spectrometer coupled with an Agilent 1290 series HPLC
1048 system for assessment of all other lipid species (Huynh et al., 2019). Lipids run on the
1049 Agilent 6490 were measured using scheduled multiple reaction monitoring with the following
1050 conditions: isolation widths for Q1 and Q3 were set to "unit" resolution (0.7 amu), gas
1051 temperature 150°C, nebulizer 20 psi, sheath gas temperature 200°C, gas flow rate 17 L/min,
1052 capillary voltage 3500 V and sheath gas flow 10 L/min. The list of MRMs used and the
1053 chromatographic conditions were described previously (Huynh et al., 2019).

1054 *Bioinformatic analysis of lipidomics data.* For lipidomics we identified that the increase in
1055 CLs in the un-normalized data was due to a training-induced increase in MPE in our
1056 mitochondrial isolates. To eliminate this bias, all lipid species were normalized by total CL
1057 amount (Table S8). Lipid species were log transformed before undergoing differential
1058 expression analysis in *limma* (Ritchie et al., 2015), with linear models using the eBayes
1059 function. The resulting differential expression values were filtered for an adjusted P value <
1060 0.05 using Benjamini Hochberg method (Table S9). Heatmaps were visualized using
1061 hierarchical clustering using the "complete" method. Profile plots were determined by taking
1062 the mean of the z-score for all participants' samples for each lipid species at each time point

1063 (Figure 4D). Forest plots are depicted using logFC results from *Limma* analysis (Figure S3).
1064 Higher classes were determined through descriptions of the literature as assigned by the Lipid
1065 Metabolites and Pathways Strategy (Lipid MAPS) (Fahy et al., 2011).

1066 **QUANTIFICATION AND STATISTICAL ANALYSIS**

1067 All values are reported as means ± SD, unless otherwise specified. For non-omics analyses:
1068 outliers were first removed using the ROUT method set at Q = 1% (Motulsky and Brown,
1069 2006). Normally distributed datasets (Shapiro-Wilk test $P > 0.05$) were analyzed by a
1070 repeated measures one-way ANOVA followed by Tukey's correction post hoc testing. Non-
1071 normally distributed datasets (Shapiro-Wilk test $P < 0.05$) were transformed using, in order,
1072 log(Y), 1/Y, √Y, until normality was met, before being analyzed as above; datasets that
1073 remained non-normal following 3 independent transformation attempts were analyzed using
1074 the non-parametric Friedman test on the raw data followed by Dunn's correction post hoc
1075 testing. The level of statistical significance was set a priori at $P < 0.05$. GraphPad Prism (v.
1076 8.4.2) was used for all statistical non-omics analyses. Differential expression for all omics
1077 was completed in R (v.3.6.3), using the packages, limma and edgeR to determine
1078 significantly enriched results between the groups. Significance was determined by an
1079 adjusted p value < 0.05 for the transcriptomics and lipidomics and 0.01 for the proteomics.
1080 Statistical details can be found in the associated figure legends.

1081 **REFERENCES**

1082 Baldwin, J., Snow, R.J., and Febbraio, M.A. (2000). Effect of training status and relative
1083 exercise intensity on physiological responses in men. Med. Sci. Sports Exerc. *32*, 1648-1654.

1084 Barnard, R.J., Edgerton, V.R., and Peter, J. (1970). Effect of exercise on skeletal muscle. I.
1085 Biochemical and histochemical properties. J. Appl. Physiol. *28*, 762-766.

1086 Benador, I.Y., Veliova, M., Liesa, M., and Shirihai, O.S. (2019). Mitochondria bound to lipid
1087 droplets: where mitochondrial dynamics regulate lipid storage and utilization. Cell Metab. *29*,
1088 827-835.

1089 Bishop, D.J., Botella, J., Genders, A.J., Lee, M.J.-C., Saner, N.J., Kuang, J., Yan, X., and
1090 Granata, C. (2019). High-Intensity Exercise and Mitochondrial Biogenesis: Current
1091 Controversies and Future Research Directions. Physiology *34*, 56-70.

1092 Bishop, D.J., Granata, C., and Eynon, N. (2014). Can we optimise the exercise training
1093 prescription to maximise improvements in mitochondria function and content? Biochim.
1094 Biophys. Acta, Gen. Subj. *1840*, 1266-1275.

1095 Bishop, D.J., Jenkins, D.G., McEniery, M., and Carey, M.F. (2000). Relationship between
1096 plasma lactate parameters and muscle characteristics in female cyclists. Med. Sci. Sports
1097 Exerc. *32*, 1088-1093.

1098 Booth, F.W., Gordon, S.E., Carlson, C.J., and Hamilton, M.T. (2000). Waging war on
1099 modern chronic diseases: primary prevention through exercise biology. J. Appl. Physiol. *88*,
1100 774-787.

1101 Bruce, C.R., Thrush, A.B., Mertz, V.A., Bezaire, V., Chabowski, A., Heigenhauser, G.J.F.,
1102 and Dyck, D.J. (2006). Endurance training in obese humans improves glucose tolerance and
1103 mitochondrial fatty acid oxidation and alters muscle lipid content. American Journal of
1104 Physiology - Endocrinology and Metabolism *291*, E99-E107.

1105 Calvo, S.E., Clauser, K.R., and Mootha, V.K. (2016). MitoCarta2.0: an updated inventory of
1106 mammalian mitochondrial proteins. Nucleic Acids Res. *44*, D1251-1257.

1107 Chen, E.Y., Tan, C.M., Kou, Y., Duan, Q., Wang, Z., Meirelles, G.V., Clark, N.R., and
1108 Ma'ayan, A. (2013). Enrichr: interactive and collaborative HTML5 gene list enrichment
1109 analysis tool. BMC Bioinformatics *14*, 128.

1110 Cox, J., and Mann, M. (2008). MaxQuant enables high peptide identification rates,
1111 individualized ppb-range mass accuracies and proteome-wide protein quantification. Nat.
1112 Biotechnol. *26*, 1367-1372.

1113 Cox, J., Neuhauser, N., Michalski, A., Scheltema, R.A., Olsen, J.V., and Mann, M. (2011).
1114 Andromeda: a peptide search engine integrated into the MaxQuant environment. J. Proteome
1115 Res. *10*, 1794-1805.

1116 Desler, C., Hansen, T.L., Frederiksen, J.B., Marcker, M.L., Singh, K.K., and Juel Rasmussen,
1117 L. (2012). Is there a link between mitochondrial reserve respiratory capacity and aging?
1118 Journal of aging research *2012*.

1119 Dube, J., Amati, F., Toledo, F., Stefanovic-Racic, M., Rossi, A., Coen, P., and Goodpaster, B.
1120 (2011). Effects of weight loss and exercise on insulin resistance, and intramyocellular
1121 triacylglycerol, diacylglycerol and ceramide. Diabetologia *54*, 1147-1156.

1122 Egan, B., Dowling, P., O'Connor, P.L., Henry, M., Meleady, P., Zierath, J.R., and O'Gorman,
1123 D.J. (2011). 2-D DIGE analysis of the mitochondrial proteome from human skeletal muscle
1124 reveals time course-dependent remodelling in response to 14 consecutive days of endurance
1125 exercise training. Proteomics *11*, 1413-1428.

1126 Ehses, S., Raschke, I., Mancuso, G., Bernacchia, A., Geimer, S., Tondera, D., Martinou, J.-
1127 C., Westermann, B., Rugarli, E.I., and Langer, T. (2009). Regulation of OPA1 processing and
1128 mitochondrial fusion by m-AAA protease isoenzymes and OMA1. J. Cell Biol. *187*, 1023-
1129 1036.

1130 Eramo, M.J., Lisnyak, V., Formosa, L.E., and Ryan, M.T. (2020). The 'mitochondrial contact
1131 site and cristae organising system'(MICOS) in health and human disease. The Journal of
1132 Biochemistry *167*, 243-255.

1133 Fahy, E., Cotter, D., Sud, M., and Subramaniam, S. (2011). Lipid classification, structures
1134 and tools. Biochimica et Biophysica Acta (BBA)-Molecular and Cell Biology of Lipids *1811*,
1135 637-647.

1136 Finocchiaro, G., Ito, M., and Tanaka, K. (1987). Purification and properties of short chain
1137 acyl-CoA, medium chain acyl-CoA, and isovaleryl-CoA dehydrogenases from human liver. J.
1138 Biol. Chem. *262*, 7982-7989.

1139 Franko, A., Baris, O.R., Bergschneider, E., Von Toerne, C., Hauck, S.M., Aichler, M.,
1140 Walch, A.K., Wurst, W., Wiesner, R.J., and Johnston, I.C. (2013). Efficient isolation of pure
1141 and functional mitochondria from mouse tissues using automated tissue disruption and
1142 enrichment with anti-TOM22 magnetic beads. PLoS One *8*, e82392.

1143 Frazier, A.E., Vincent, A.E., Turnbull, D.M., Thorburn, D.R., and Taylor, R.W. (2020).
1144 Assessment of mitochondrial respiratory chain enzymes in cells and tissues. In Methods Cell
1145 Biol. (Elsevier), pp. 121-156.

1146 Frezza, C., Cipolat, S., and Scorrano, L. (2007). Organelle isolation: functional mitochondria
1147 from mouse liver, muscle and cultured filroblasts. Nat. Protoc. *2*, 287.

1148 Fujikawa, M., Ohsakaya, S., Sugawara, K., and Yoshida, M. (2014). Population of ATP
1149 synthase molecules in mitochondria is limited by available 6.8-kDa proteolipid protein
1150 (MLQ). Genes Cells *19*, 153-160.

1151 Gebert, N., Joshi, A.S., Kutik, S., Becker, T., McKenzie, M., Guan, X.L., Mooga, V.P.,
1152 Stroud, D.A., Kulkarni, G., and Wenk, M.R. (2009). Mitochondrial cardiolipin involved in
1153 outer-membrane protein biogenesis: implications for Barth syndrome. Curr. Biol. *19*, 2133-
1154 2139.

1155 Goodpaster, B.H., and Kelley, D.E. (1998). Role of muscle in triglyceride metabolism. Curr.
1156 Opin. Lipidol. *9*, 231-236.

1157 Gorman, G.S., Chinnery, P.F., DiMauro, S., Hirano, M., Koga, Y., McFarland, R.,
1158 Suomalainen, A., Thorburn, D.R., Zeviani, M., and Turnbull, D.M. (2016). Mitochondrial
1159 diseases. Nature reviews Disease primers *2*, 1-22.

1160 Granata, C., Jamnick, N.A., and Bishop, D.J. (2018a). Principles of exercise prescription, and
1161 how they influence exercise-induced changes of transcription factors and other regulators of
1162 mitochondrial biogenesis. Sports Med. *48*, 1541–1559.

1163 Granata, C., Jamnick, N.A., and Bishop, D.J. (2018b). Training-induced changes in
1164 mitochondrial content and respiratory function in human skeletal muscle. Sports Med. *48*,
1165 1809–1828.

1166 Granata, C., Oliveira, R.S.F., Little, J.P., Renner, K., and Bishop, D.J. (2016a). Mitochondrial
1167 adaptations to high-volume exercise training are rapidly reversed after a reduction in training
1168 volume in human skeletal muscle. FASEB J. *30*, 3413-3423.

1169 Granata, C., Oliveira, R.S.F., Little, J.P., Renner, K., and Bishop, D.J. (2016b). Training
1170 intensity modulates changes in PGC-1α and p53 protein content and mitochondrial
1171 respiration, but not markers of mitochondrial content in human skeletal muscle. FASEB J. *30*,
1172 959-970.

1173 Greggio, C., Jha, P., Kulkarni, S.S., Lagarrigue, S., Broskey, N.T., Boutant, M., Wang, X.,
1174 Alonso, S.C., Ofori, E., and Auwerx, J. (2017). Enhanced respiratory chain supercomplex
1175 formation in response to exercise in human skeletal muscle. Cell Metab. *25*, 301-311.

1176 Groennebaek, T., Nielsen, J., Jespersen, N.R., Bøtker, H.E., de Paoli, F.V., Miller, B.F., and
1177 Vissing, K. (2020). Utilization of biomarkers as predictors of skeletal muscle mitochondrial
1178 content after physiological intervention and in clinical settings. American Journal Of
1179 Physiology-Endocrinology And Metabolism *318*, E886-E889.

1180 Guarani, V., McNeill, E.M., Paulo, J.A., Huttlin, E.L., Fröhlich, F., Gygi, S.P., Van Vactor,
1181 D., and Harper, J.W. (2015). QIL1 is a novel mitochondrial protein required for MICOS
1182 complex stability and cristae morphology. Elife *4*, e06265.

1183 Hirst, J. (2018). Open questions: respiratory chain supercomplexes—why are they there and
1184 what do they do? BMC Biol. *16*, 111.

1185 Hock, D.H., Robinson, D.R., and Stroud, D.A. (2020). Blackout in the powerhouse: clinical
1186 phenotypes associated with defects in the assembly of OXPHOS complexes and the
1187 mitoribosome. Biochem. J. *477*, 4085-4132.

1188 Holloszy, J.O. (1967). Biochemical adaptations in muscle. Effects of exercise on
1189 mitochondrial oxygen uptake and respiratory enzyme activity in skeletal muscle. J. Biol.
1190 Chem. *242*, 2278-2282.

1191 Holloway, K.V., O'Gorman, M., Woods, P., Morton, J.P., Evans, L., Cable, N.T., Goldspink,
1192 D.F., and Burniston, J.G. (2009). Proteomic investigation of changes in human vastus
1193 lateralis muscle in response to interval-exercise training. Proteomics *9*, 5155-5174.

1194 Hoppeler, H., Lüthi, P., Claassen, H., Weibel, E.R., and Howald, H. (1973). The
1195 ultrastructure of the normal human skeletal muscle. Pflügers Archiv *344*, 217-232.

1196 Hostrup, M., Onslev, J., Jacobson, G.A., Wilson, R., and Bangsbo, J. (2018). Chronic β2-
1197 adrenoceptor agonist treatment alters muscle proteome and functional adaptations induced by
1198 high intensity training in young men. The Journal of physiology *596*, 231-252.

1199 Huynen, M.A., Mühlmeister, M., Gotthardt, K., Guerrero-Castillo, S., and Brandt, U. (2016).
1200 Evolution and structural organization of the mitochondrial contact site (MICOS) complex and
1201 the mitochondrial intermembrane space bridging (MIB) complex. Biochimica et Biophysica
1202 Acta (BBA)-Molecular Cell Research *1863*, 91-101.

1203 Huynh, K., Barlow, C.K., Jayawardana, K.S., Weir, J.M., Mellett, N.A., Cinel, M., Magliano,
1204 D.J., Shaw, J.E., Drew, B.G., and Meikle, P.J. (2019). High-throughput plasma lipidomics:
1205 detailed mapping of the associations with cardiometabolic risk factors. Cell chemical biology
1206 *26*, 71-84. e74.

1207 Ikon, N., and Ryan, R.O. (2017). Cardiolipin and mitochondrial cristae organization.
1208 Biochimica et Biophysica Acta (BBA)-Biomembranes *1859*, 1156-1163.

1209 Jamnick, N.A., Botella, J., Pyne, D.B., and Bishop, D.J. (2018). Manipulating graded
1210 exercise test variables affects the validity of the lactate threshold and V˙ O2peak. PLoS One
1211 *13*, e0199794.

1212 Jha, P., Wang, X., and Auwerx, J. (2016). Analysis of Mitochondrial Respiratory Chain
1213 Supercomplexes Using Blue Native Polyacrylamide Gel Electrophoresis (BN-PAGE). Curr.
1214 Protoc. Mouse Biol., 1-14.

1215 Kampjut, D., and Sazanov, L.A. (2019). Structure and mechanism of mitochondrial proton-
1216 translocating transhydrogenase. Nature *573*, 291-295.

1217 Kulak, N.A., Pichler, G., Paron, I., Nagaraj, N., and Mann, M. (2014). Minimal, encapsulated
1218 proteomic-sample processing applied to copy-number estimation in eukaryotic cells. Nature
1219 methods *11*, 319.

1220 Kuleshov, M.V., Jones, M.R., Rouillard, A.D., Fernandez, N.F., Duan, Q., Wang, Z., Koplev,
1221 S., Jenkins, S.L., Jagodnik, K.M., and Lachmann, A. (2016). Enrichr: a comprehensive gene
1222 set enrichment analysis web server 2016 update. Nucleic Acids Res. *44*, W90-W97.

1223 LaHue, S.C., Comella, C.L., and Tanner, C.M. (2016). The best medicine? The influence of
1224 physical activity and inactivity on Parkinson's disease. Mov. Disord. *31*, 1444-1454.

1225 Lapuente-Brun, E., Moreno-Loshuertos, R., Acín-Pérez, R., Latorre-Pellicer, A., Colás, C.,
1226 Balsa, E., Perales-Clemente, E., Quirós, P.M., Calvo, E., and Rodríguez-Hernández, M.
1227 (2013). Supercomplex assembly determines electron flux in the mitochondrial electron
1228 transport chain. Science *340*, 1567-1570.

1229 Larsen, S., Nielsen, J., Hansen, C.N., Nielsen, L.B., Wibrand, F., Stride, N., Schroder, H.D.,
1230 Boushel, R., Helge, J.W., Dela, F., et al. (2012). Biomarkers of mitochondrial content in
1231 skeletal muscle of healthy young human subjects. J. Physiol. *590*, 3349-3360.

1232 Lazar, C. imputeLCMD: A Collection of Methods for Left-Censored Missing Data
1233 Imputation. R package, version 2.0.

1234 Lin, M.T., and Beal, M.F. (2006). Mitochondrial dysfunction and oxidative stress in
1235 neurodegenerative diseases. Nature *443*, 787-795.

1236 López-Otín, C., Blasco, M.A., Partridge, L., Serrano, M., and Kroemer, G. (2013). The
1237 hallmarks of aging. Cell *153*, 1194-1217.

1238 Malhotra, A., Xu, Y., Ren, M., and Schlame, M. (2009). Formation of molecular species of
1239 mitochondrial cardiolipin. 1. A novel transacylation mechanism to shuttle fatty acids between
1240 sn-1 and sn-2 positions of multiple phospholipid species. Biochimica et Biophysica Acta
1241 (BBA)-Molecular and Cell Biology of Lipids *1791*, 314-320.

1242 Martínez-Reyes, I., and Chandel, N.S. (2020). Mitochondrial TCA cycle metabolites control
1243 physiology and disease. Nature communications *11*, 1-11.

1244 McKenzie, M., Lazarou, M., Thorburn, D.R., and Ryan, M.T. (2007). Analysis of
1245 mitochondrial subunit assembly into respiratory chain complexes using Blue Native
1246 polyacrylamide gel electrophoresis. Anal. Biochem. *364*, 128-137.

1247 Meinild Lundby, A.K., Jacobs, R.A., Gehrig, S., de Leur, J., Hauser, M., Bonne, T.C., Flück,
1248 D., Dandanell, S., Kirk, N., Kaech, A., et al. (2018). Exercise training increases skeletal
1249 muscle mitochondrial volume density by enlargement of existing mitochondria and not de
1250 novo biogenesis. Acta Physiol *222*, e12905.

1251 Morgan, T., Cobb, L., Short, F., Ross, R., and Gunn, D. (1971). Effects of long-term exercise
1252 on human muscle mitochondria. In Muscle metabolism during exercise (Springer), pp. 87-95.

1253 Motulsky, H.J., and Brown, R.E. (2006). Detecting outliers when fitting data with nonlinear
1254 regression–a new method based on robust nonlinear regression and the false discovery rate.
1255 BMC Bioinformatics *7*, 123.

1256 Mráček, T., Drahota, Z., and Houštěk, J. (2013). The function and the role of the
1257 mitochondrial glycerol-3-phosphate dehydrogenase in mammalian tissues. Biochimica et
1258 Biophysica Acta (BBA)-Bioenergetics *1827*, 401-410.

1259 Neufer, P.D., Bamman, M.M., Muoio, D.M., Bouchard, C., Cooper, D.M., Goodpaster, B.H.,
1260 Booth, F.W., Kohrt, W.M., Gerszten, R.E., Mattson, M.P., et al. (2015). Understanding the
1261 cellular and molecular mechanisms of physical activity-induced health benefits. Cell Metab.
1262 *22*, 4-11.

1263 Nielsen, J., Gejl, K.D., Hey-Mogensen, M., Holmberg, H.C., Suetta, C., Krustrup, P.,
1264 Elemans, C.P., and Ørtenblad, N. (2017). Plasticity in mitochondrial cristae density allows
1265 metabolic capacity modulation in human skeletal muscle. J. Physiol. *595*, 2839-2847.

1266 Nunnari, J., and Suomalainen, A. (2012). Mitochondria: in sickness and in health. Cell *148*,
1267 1145-1159.

1268 Oldham, W.M., Clish, C.B., Yang, Y., and Loscalzo, J. (2015). Hypoxia-mediated increases
1269 in L-2-hydroxyglutarate coordinate the metabolic response to reductive stress. Cell Metab.
1270 *22*, 291-303.

1271 Ørtenblad, N. (2018). Mitochondrial increase in volume density with exercise training: More,
1272 larger or better? Acta Physiologica *222*, e12976.

1273 Palmieri, F. (2013). The mitochondrial transporter family SLC25: identification, properties
1274 and physiopathology. Mol. Aspects Med. *34*, 465-484.

1275 Pedersen, B.K., and Saltin, B. (2006). Evidence for prescribing exercise as therapy in chronic
1276 disease. Scand. J. Med. Sci. Sports *16*, 3-63.

1277 Perreault, L., Newsom, S.A., Strauss, A., Kerege, A., Kahn, D.E., Harrison, K.A., Snell-
1278 Bergeon, J.K., Nemkov, T., D'Alessandro, A., and Jackman, M.R. (2018). Intracellular
1279 localization of diacylglycerols and sphingolipids influences insulin sensitivity and
1280 mitochondrial function in human skeletal muscle. JCI insight *3*.

1281 Pesta, D., and Gnaiger, E. (2012). High-resolution respirometry: OXPHOS protocols for
1282 human cells and permeabilized fibers from small biopsies of human muscle. In Mitochondrial
1283 Bioenergetics: Methods and Protocols. C.M. Palmeira, and A.J. Moreno, eds. (Springer
1284 Science+Business Media), pp. 25-58.

1285 Pfeiffer, K., Gohil, V., Stuart, R.A., Hunte, C., Brandt, U., Greenberg, M.L., and Schägger,
1286 H. (2003). Cardiolipin stabilizes respiratory chain supercomplexes. J. Biol. Chem. *278*,
1287 52873-52880.

1288 Pillon, N.J., Gabriel, B.M., Dollet, L., Smith, J.A., Puig, L.S., Botella, J., Bishop, D.J.,
1289 Krook, A., and Zierath, J.R. (2020). Transcriptomic profiling of skeletal muscle adaptations
1290 to exercise and inactivity. Nature communications *11*, 1-15.

1291 Powers, S.K., Deminice, R., Ozdemir, M., Yoshihara, T., Bomkamp, M.P., and Hyatt, H.
1292 (2020). Exercise-induced oxidative stress: Friend or foe? Journal of sport and health science.

1293 Ritchie, M.E., Phipson, B., Wu, D., Hu, Y., Law, C.W., Shi, W., and Smyth, G.K. (2015).
1294 limma powers differential expression analyses for RNA-sequencing and microarray studies.
1295 Nucleic Acids Res. *43*, e47-e47.

1296 Robinson, M.M., Dasari, S., Konopka, A.R., Johnson, M.L., Manjunatha, S., Esponda, R.R.,
1297 Carter, R.E., Lanza, I.R., and Nair, K.S. (2017). Enhanced protein translation underlies
1298 improved metabolic and physical adaptations to different exercise training modes in young
1299 and old humans. Cell Metab. *25*, 581-592.

1300 Scalzo, R.L., Peltonen, G.L., Binns, S.E., Shankaran, M., Giordano, G.R., Hartley, D.A.,
1301 Klochak, A.L., Lonac, M.C., Paris, H.L.R., Szallar, S.E., et al. (2014). Greater muscle protein
1302 synthesis and mitochondrial biogenesis in males compared with females during sprint interval
1303 training. FASEB J. *28*, 2705-2714.

1304 Schägger, H., and Pfeiffer, K. (2000). Supercomplexes in the respiratory chains of yeast and
1305 mammalian mitochondria. The EMBO journal *19*, 1777-1783.

1306 Schulz, H. (1991). Beta oxidation of fatty acids. Biochimica et Biophysica Acta (BBA)-
1307 Lipids and Lipid Metabolism *1081*, 109-120.

1308 Shankaran, M., King, C.L., Angel, T.E., Holmes, W.E., Li, K.W., Colangelo, M., Price, J.C.,
1309 Turner, S.M., Bell, C., and Hamilton, K.L. (2016). Circulating protein synthesis rates reveal
1310 skeletal muscle proteome dynamics. The Journal of clinical investigation *126*, 288-302.

1311 Shepherd, S., Cocks, M., Meikle, P., Mellett, N., Ranasinghe, A., Barker, T., Wagenmakers,
1312 A., and Shaw, C. (2017). Lipid droplet remodelling and reduced muscle ceramides following
1313 sprint interval and moderate-intensity continuous exercise training in obese males. Int. J.
1314 Obes. *41*, 1745.

1315 Signes, A., and Fernandez-Vizarra, E. (2018). Assembly of mammalian oxidative
1316 phosphorylation complexes I–V and supercomplexes. Essays Biochem. *62*, 255-270.

1317 Smith, A.C., and Robinson, A.J. (2019). MitoMiner v4. 0: an updated database of
1318 mitochondrial localization evidence, phenotypes and diseases. Nucleic Acids Res. *47*, D1225-
1319 D1228.

1320 Spinelli, J.B., and Haigis, M.C. (2018). The multifaceted contributions of mitochondria to
1321 cellular metabolism. Nat. Cell Biol. *20*, 745-754.

1322 Stefely, J.A., and Pagliarini, D.J. (2017). Biochemistry of mitochondrial coenzyme Q
1323 biosynthesis. Trends Biochem. Sci. *42*, 824-843.

1324 Stroud, D.A., Surgenor, E.E., Formosa, L.E., Reljic, B., Frazier, A.E., Dibley, M.G.,
1325 Osellame, L.D., Stait, T., Beilharz, T.H., and Thorburn, D.R. (2016). Accessory subunits are
1326 integral for assembly and function of human mitochondrial complex I. Nature *538*, 123.

1327 Svensson, M., Malm, C., Tonkonogi, M., Ekblom, B., Sjödin, B., and Sahlin, K. (1999).
1328 Effect of Q10 supplementation on tissue Q10 levels and adenine nucleotide catabolism during
1329 high-intensity exercise. Int. J. Sport Nutr. Exerc. Metab. *9*, 166-180.

1330 Takai, Y., Sasaki, T., and Matozaki, T. (2001). Small GTP-binding proteins. Physiol. Rev.
1331 *81*, 153-208.

1332 Tan, S.M., Ziemann, M., Thallas-Bonke, V., Snelson, M., Kumar, V., Laskowski, A.,
1333 Nguyen, T.-V., Huynh, K., Clarke, M.V., and Libianto, R. (2020). Complement C5a Induces
1334 Renal Injury in Diabetic Kidney Disease by Disrupting Mitochondrial Metabolic Agility.
1335 Diabetes *69*, 83-98.

1336 Ubaida-Mohien, C., Gonzalez-Freire, M., Lyashkov, A., Moaddel, R., Chia, C.W.,
1337 Simonsick, E.M., Sen, R., and Ferrucci, L. (2019). Physical activity associated proteomics of
1338 skeletal muscle: being physically active in daily life may protect skeletal muscle from aging.
1339 Front. Physiol. *10*, 312.

1340 Voos, W. (2013). Chaperone–protease networks in mitochondrial protein homeostasis.
1341 Biochimica et Biophysica Acta (BBA)-Molecular Cell Research *1833*, 388-399.

1342 Walther, T.C., and Farese Jr, R.V. (2012). Lipid droplets and cellular lipid metabolism.
1343 Annu. Rev. Biochem. *81*, 687-714.

1344 Wang, H., Sreenivasan, U., Hu, H., Saladino, A., Polster, B.M., Lund, L.M., Gong, D.-w.,
1345 Stanley, W.C., and Sztalryd, C. (2011). Perilipin 5, a lipid droplet-associated protein,
1346 provides physical and metabolic linkage to mitochondria. J. Lipid Res. *52*, 2159-2168.

1347 Wang, Y., and Hekimi, S. (2016). Understanding ubiquinone. Trends Cell Biol. *26*, 367-378.

1348 Wang, Y., and Hekimi, S. (2019). The complexity of making ubiquinone. Trends Endocrinol.
1349 Metab. *30*, 929-943.

1350 Watmough, N.J., and Frerman, F.E. (2010). The electron transfer flavoprotein: ubiquinone
1351 oxidoreductases. Biochimica et Biophysica Acta (BBA)-Bioenergetics *1797*, 1910-1916.

1352 Weber, T.A., Koob, S., Heide, H., Wittig, I., Head, B., van der Bliek, A., Brandt, U.,
1353 Mittelbronn, M., and Reichert, A.S. (2013). APOOL is a cardiolipin-binding constituent of
1354 the Mitofilin/MINOS protein complex determining cristae morphology in mammalian
1355 mitochondria. PLoS One *8*, e63683.

1356 Weir, J.M., Wong, G., Barlow, C.K., Greeve, M.A., Kowalczyk, A., Almasy, L., Comuzzie,
1357 A.G., Mahaney, M.C., Jowett, J.B., and Shaw, J. (2013). Plasma lipid profiling in a large
1358 population-based cohort. J. Lipid Res. *54*, 2898-2908.

1359 Wiedemann, N., and Pfanner, N. (2017). Mitochondrial machineries for protein import and
1360 assembly. Annu. Rev. Biochem. *86*, 685-714.

1361 Wyckelsma, V.L., Levinger, I., McKenna, M.J., Formosa, L.E., Ryan, M.T., Petersen, A.C.,
1362 Anderson, M.J., and Murphy, R.M. (2017). Preservation of skeletal muscle mitochondrial
1363 content in older adults: relationship between mitochondria, fibre type and high-intensity
1364 exercise training. The Journal of physiology *595*, 3345-3359.

1365 Xia, L., Björnstedt, M., Nordman, T., Eriksson, L.C., and Olsson, J.M. (2001). Reduction of
1366 ubiquinone by lipoamide dehydrogenase: An antioxidant regenerating pathway. Eur. J.
1367 Biochem. *268*, 1486-1490.

1368